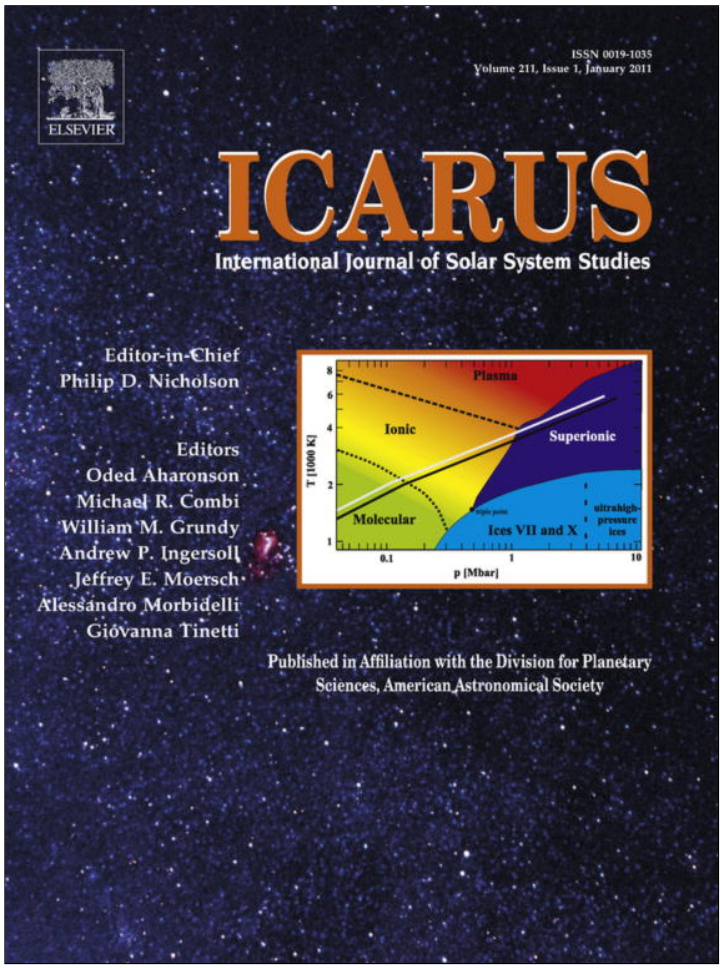

(This is a sample cover image for this issue. The actual cover is not yet available at this time.)

Icarus 216 (2011) 89–110

Contents lists available at SciVerse ScienceDirect

Icarus

journal homepage: www.elsevier.com/locate/icarus

Titan's cloud seasonal activity from winter to spring with Cassini/VIMS

S. Rodriguez [a,*], S. Le Mouélic [b], P. Rannou [c], C. Sotin [b,d], R.H. Brown [e], J.W. Barnes [f], C.A. Griffith [e], J. Burgalat [c], K.H. Baines [g], B.J. Buratti [d], R.N. Clark [h], P.D. Nicholson [i]

[a] Laboratoire AIM, Université Paris Diderot, Paris 7/CNRS/CEA-Saclay, DSM/IRFU/SAp, Centre de l'Orme des Merisiers, bât. 709, 91191 Gif sur Yvette, France
[b] Laboratoire de Planétologie et Géodynamique, UMR CNRS 6112, Université de Nantes, 2 rue de la Houssinière, BP 92205, 44322 Nantes Cedex 3, France
[c] Groupe de Spectroscopie Moléculaire et Atmosphérique, UMR CNRS 6089, Université de Reims, U.F.R. Sciences Exactes et Naturelles, Moulin de la Housse, BP 1039, 51687 Reims Cedex 2, France
[d] Jet Propulsion Laboratory, 4800 Oak Grove Drive, Pasadena, CA 91109, USA
[e] Lunar and Planetary Lab and Stewart Observatory, University of Arizona, 1629 E. University Blvd., Tucson, AZ 85721-0092, USA
[f] Department of Physics, University of Idaho, Engineering-Physics Building, Moscow, ID 83844, USA
[g] Space Science and Engineering Center, University of Wisconsin-Madison, 1225 West Dayton St., Madison, WI 53706, USA
[h] US Geological Survey, Denver Federal Center, Denver, CO 80225-0046, USA
[i] Cornell University, 418 Space Sciences Building, Ithaca, NY 14853, USA

ARTICLE INFO

Article history:
Received 21 November 2010
Revised 13 July 2011
Accepted 25 July 2011
Available online 5 August 2011

Keywords:
Satellites, Atmospheres
Titan
Meteorology

ABSTRACT

Since Saturn orbital insertion in July 2004, the Cassini orbiter has been observing Titan throughout most of the northern winter season (October 2002–August 2009) and the beginning of spring, allowing a detailed monitoring of Titan's cloud coverage at high spatial resolution with close flybys on a monthly basis. This study reports on the analysis of all the near-infrared images of Titan's clouds acquired by the Visual and Infrared Mapping Spectrometer (VIMS) during 67 targeted flybys of Titan between July 2004 and April 2010.

The VIMS observations show numerous sporadic clouds at southern high and mid-latitudes, rare clouds in the equatorial region, and reveal a long-lived cloud cap above the north pole, ubiquitous poleward of 60°N. These observations allow us to follow the evolution of the cloud coverage during almost a 6-year period including the equinox, and greatly help to further constrain global circulation models (GCMs). After 4 years of regular outbursts observed by Cassini between 2004 and 2008, southern polar cloud activity started declining, and completely ceased 1 year before spring equinox. The extensive cloud system over the north pole, stable between 2004 and 2008, progressively fractionated and vanished as Titan entered into northern spring. At southern mid-latitudes, clouds were continuously observed throughout the VIMS observing period, even after equinox, in a latitude band between 30°S and 60°S. During the whole period of observation, only a dozen clouds were observed closer to the equator, though they were slightly more frequent as equinox approached.

We also investigated the distribution of clouds with longitude. We found that southern polar clouds, before disappearing in mid-2008, were systematically concentrated in the leading hemisphere of Titan, in particular above and to the east of Ontario Lacus, the largest reservoir of hydrocarbons in the area. Clouds are also non-homogeneously distributed with longitude at southern mid-latitudes. The $n = 2$-mode wave pattern of the distribution, observed since 2003 by Earth-based telescopes and confirmed by our Cassini observations, may be attributed to Saturn's tides.

Although the latitudinal distribution of clouds is now relatively well reproduced and understood by the GCMs, the non-homogeneous longitudinal distributions and the evolution of the cloud coverage with seasons still need investigation. If the observation of a few single clouds at the tropics and at northern mid-latitudes late in winter and at the start of spring cannot be further interpreted for the moment, the obvious shutdown of the cloud activity at Titan's poles provides clear signs of the onset of the general circulation turnover that is expected to accompany the beginning of Titan's northern spring. According to our GCM, the persistence of clouds at certain latitudes rather suggests a 'sudden' shift in near future of the meteorology into the more illuminated hemisphere. Finally, the observed seasonal change in cloud activity occurred with a significant time lag that is not predicted by our model. This may be due to an overall methane humidity at Titan's surface higher than previously expected.

* Corresponding author. Fax: +33 (0)1 69 08 65 77.
E-mail address: sebastien.rodriguez@cea.fr (S. Rodriguez).

0019-1035/$ - see front matter © 2011 Elsevier Inc. All rights reserved.
doi:10.1016/j.icarus.2011.07.031

1. Introduction

Titan is the only moon in the Solar System with a dense atmosphere. Its atmospheric dynamics are driven by latitudinal temperature differences and seasonal temperature variations. Saturn has an inclination of 26° relative to its orbital plane. This largest satellite of Saturn has a near-equatorial orbit and, like Saturn, has seasons about 30 times longer than those on Earth. During northern winter, the south pole is always illuminated whereas the north pole is not, resulting in a temperature difference generating an atmospheric circulation globally from the southern hemisphere to the northern hemisphere. The circulation takes the form of a Hadley cell in the troposphere, which most of the time has an ascending branch near 30–40° in the summer hemisphere, subsiding near the polar regions (Tokano et al., 2001; Tokano, 2005; Rannou et al., 2006; Mitchell et al., 2006, 2009). In the stratosphere, the circulation takes the form of a single direct cell with a broad ascending branch in the summer hemisphere and a descending branch well confined in the winter polar region.

Titan's nitrogen-laden atmosphere contains the trace condensable gas methane with a mixing ratio of about 1.65% overall, but increasing to 5% close to the surface at the Huygens landing site (Fulchignoni et al., 2005; Tomasko et al., 2005), where conditions are close to the methane triple point. This situation is similar to that of H_2O on Earth, with liquid methane possibly filling the lakes imaged by the RADAR instrument (Stofan et al., 2007). Flows of liquid methane are also thought to have carved plateaus and valley networks, such as the ones observed by the Huygens probe during its descent (Soderblom et al., 2007). Pure methane cannot be solid at the surface because the surface temperature is quite homogeneous and slightly above its freezing point (Jennings et al., 2009). However, methane could be trapped as methane clathrates. Methane is thus thought to play a central role in the moon's atmospheric activity and meteorological cycle. Methane can form clouds, possibly rain down, and collect on the surface and in sub-surface reservoirs that may then evaporate back to the atmosphere (Flasar, 1998; Tokano et al., 2001; Tokano, 2005; Atreya et al., 2006; Rannou et al., 2006; Mitchell et al., 2006, 2009). Ethane is methane's major organic photochemical byproduct (Yung et al., 1984; Toublanc et al., 1995). Liquid ethane has been identified in Ontario Lacus probably in solution with liquid methane and other lower-molecular-mass hydrocarbons and nitriles (Brown et al., 2008). Slightly less volatile than methane, ethane is therefore thought to participate to a lesser extent in the liquids/solids cycle on Titan and also to be the major constituent of the winter high latitude lakes and clouds (Griffith et al., 2006; Rannou et al., 2006; Le Mouélic et al., 2011). Both methane and ethane have the potential to form clouds.

The first detections of transient cloud activity in Titan's atmosphere were achieved thanks to spectroscopy and multispectral imaging from ground-based telescopes. The atmosphere of Titan is opaque at visible and infrared wavelengths, except for some narrow spectral windows where methane absorption is the weakest (for example in the near-infrared range at $\lambda = 0.93$, 1.08, 1.27, 1.59, 2.03, 2.75 and 5 μm – Titan's so-called atmospheric infrared windows). Griffith et al. (1998) observed a significant brightening of Titan in the wings of the atmospheric windows during September 1995, which was interpreted as a ~9% cloud cover of the moon's disk. Griffith et al. (2000) also detected spectroscopic evidence for smaller scale transient clouds occurring in several nights in 1993–1999 and covering less than 1% of Titan's disk. Year 2002 marked the first report of Titan's clouds' direct imaging and localization (Brown et al., 2002). Images were regularly obtained between 1996 and 2006 using Gemini and Keck adaptive optics facilities (Brown et al., 2002; Roe et al., 2002; Gibbard et al., 2004; de Pater et al., 2006; Schaller et al., 2006a, 2006b), the Canada France Hawaii Telescope and Very Large Telescope along with adaptive optics systems (Hirtzig et al., 2006, 2007) and the Palomar Hale telescope using the JPL adaptive optics system (Bouchez and Brown, 2005). These large clouds, observed at Titan's south pole during maximum solar illumination, were at that time thought to be predominantly composed of liquid or solid methane, demonstrating for the first time the possibility of condensation and the large influence of localized seasonal moist convection in Titan's atmosphere. These investigations from ground-based observations gathered statistical constraints on Titan's cloud distribution in time and location – in particular on the variability and periodicity of outburst and dissipation of the large south polar clouds (Schaller et al., 2006a, 2006b).

Roe et al. (2005a, 2005b) reported the first detection between December 2003 and February 2005 of temperate-latitude cloud systems occurring at ~40°S. The preferential appearance of clouds at the pole and mid-latitudes in the summer (southern at that time) hemisphere is consistent with the predictions of global circulation models (GCM) and can be explained by the general circulation in Titan's atmosphere (Tokano et al., 2001; Tokano, 2005; Rannou et al., 2006; Mitchell et al., 2006, 2009). The 40°S cloud band is triggered by the ascending branch of the Hadley cell, while the south polar clouds result from the transport of methane from warm mid-latitudes to cold polar latitudes. Roe et al. (2005b) also reported a striking longitudinal clustering of mid-latitude clouds at that time and suggested a possible surface control of the cloud activity of this region, such as local geysering or cryovolcanism. Finally, Schaller et al. (2009) recently reported the Earth-based detection of a huge tropical storm.

Since July 2004, the Cassini mission has monitored Titan's clouds in unprecedented detail on a monthly basis, which is very complementary to Earth-based observations. Two optical cameras onboard Cassini have been used to image the clouds in Titan's atmosphere: (1) The Imaging Science Subsystem (ISS) is a multi-spectral camera that can observe Titan's surface and atmosphere thanks to several filters from the UV to the near-infrared (Porco, 2004), (2) the Visual and Infrared Mapping Spectrometer (VIMS) is an imaging spectrometer that acquires hyperspectral images in 352 contiguous spectral channels between 0.3 and 5.2 μm (Brown et al., 2004). Several clouds were already observed at both poles and summer mid- and low-latitudes with ISS and VIMS during the first close flybys (Porco et al., 2005; Baines et al., 2005; Griffith et al., 2005, 2006, 2009). Besides these isolated observations, statistics on the location and time of appearance of ~50 clouds observed with ISS between 2004 and 2008 are given in Turtle et al. (2009). Turtle et al. (2009) also reported detection of clouds at the tropics. The spectral dimension of the VIMS images allows the direct spectral detection of cloud signatures and gives in addition access to the altitude of the clouds and the scattering properties of their particles (Griffith et al., 2005, 2006, 2009; Rodriguez et al., 2009; Le Mouélic et al., 2011).

An accurate comparison of cloud coverage with GCM predictions requires the best available temporal and spatial statistics. The models, however, have hitherto been poorly constrained and their long-term meteorological predictions have not yet been observationally fully verified. These models (e.g. Rannou et al., 2006; Mitchell et al., 2006, 2009) differ significantly in their forecast by considering how Titan's atmospheric humidity, and therefore the cloud coverage, shifts from one hemisphere to the other with the seasons. Constraining the long-term evolution of Titan's meteorology is important to understanding if sustained cloud coverage, rain, or storms could happen in tropical regions. It can help

to appreciate if rainfalls can occur near the Huygens probe landing site in the present day to create the observed drainage channels – at the same latitudes where most of the land area is covered by presumably dry equatorial dune fields. It can also provide constrains on whether a north–south asymmetry in precipitation is present, which might then explain the asymmetry in Titan's lake distribution (Aharonson et al., 2009). The monitoring of clouds can significantly contribute to the global understanding of Titan's climate, meteorological and hydrocarbon cycles.

The previously published long-term cloud survey from VIMS runs from July 2004 to December 2007 (Rodriguez et al., 2009). More than 140 cloud events were found revealing the evolution with time of their spatial coverage during almost half a Titan season during southern summer. Although the spatial cloud coverage was in general agreement with the GCM from Rannou et al. (2006), the non-detection of isolated clouds at latitudes of ~40°N and the persistence of the southern clouds at the end of 2007 while southern summer is ending were in disagreement with the GCM (Rodriguez et al., 2009). The present paper extends the study up to 2010 and provides additional constraints for the GCMs.

After describing the semi-automated methodology that we use to detect the clouds, this paper provides time-averaged cloud coverage maps of Titan as well as latitude occurrence of clouds versus time. Our survey covers now almost one Titan season from early northern winter to the beginning of northern spring. Evolution during that season and implications for GCMs and the comprehension of Titan's climatology are discussed.

2. Semi-automatic detection of Titan's clouds within VIMS images

The VIMS imaging spectrometer observes Titan at global scale at low to medium resolution (400–25 km/pixel), and at high resolution over a few percents of the surface, up to 500 m/pixel in localized areas (e.g. Barnes et al., 2008; Le Corre et al., 2009). A complete description of the VIMS observations of Titan during the entire Cassini nominal mission (July 2004–July 2008) is available in Barnes et al. (2009). Clouds systems are clearly visible in several VIMS images at diagnostic infrared wavelengths (Baines et al., 2005; Griffith et al., 2005, 2006, 2009; Rodriguez et al., 2009; Barnes et al., 2007, 2009). Between July 2004 (flyby T0) and April 2010 (T67), VIMS acquired more than 20,000 hyperspectral images of Titan. By eliminating redundant, night side, limb viewing, very low time exposure and also very small images, we reduced the dataset down to ~2000 spectro-images useful for the purpose of cloud detection. This still represents several millions of spectra and thousands of images to inspect, preventing the efficient use of a manual detection technique alone. We therefore developed a semi-automated algorithm to detect clouds in VIMS images (Rodriguez et al., 2009). The basics of this method were already described in Rodriguez et al. (2009), and are briefly summarized here.

Because clouds are efficient reflectors in the near-infrared and substantially reduce the path-length of solar photons in Titan's atmosphere, their spectra present a significant and simultaneous relative brightening of all atmospheric windows, which is not the case for surface or limb spectra. Owing to these specific spectral signatures, the clouds on Titan can therefore be distinguished from other atmospheric or surface features (Rodriguez et al., 2009). The cloud-related brightening of the atmospheric windows mainly depends on the cloud top altitude and composition, and on the size and number density of the droplets; this spectral signature was the subject of other specific studies (Griffith et al., 2005, 2006, 2009).

We systematically analyzed several VIMS images with and without cloud features in order to derive a spectral criterion that would be specific to the cloud spectral signature only. Some specific surface features (such as Tui and Hotei Regio; i.e. Barnes et al., 2005, 2006 – see Fig. 1 in Rodriguez et al. (2009)) show a particularly bright 5 μm window with very strong signal relative to all other windows. On the other hand, cloud spectra always show simultaneous brightening of all windows, particularly at 2.75 and 5 μm (see an example in Fig. 1 from Rodriguez et al. (2009)). Taking into account the great variability of the VIMS dataset in terms of resolution, illumination, emission and phase angles, we empirically found that the most robust detection criterion to separate pixels that contain a "cloudy" spectral component from any other component is to use the simultaneous brightening of the 2.75 and 5 μm windows. We found that taking a single window or a combination of two other windows leads repeatedly to false positive detections.

We then developed an algorithm that automatically calculates the 2.75 and 5 μm window areas for every pixel of each VIMS datacube. These areas are defined as the integrals of the reflectance between 2.35 and 3.21 μm for the 2.75 μm window and between 4.74 μm and 5.11 μm for the 5 μm window. For each VIMS cube, a 2D scatter plot of areas at 5 μm versus areas at 2.75 μm is then built. In this new space of representation, most of the pixels of the cube are statistically distributed within a Gaussian shape, except for pixels with a cloud contribution that are clustered in the "high-value" wing of the distributions (see 2D scatter plot in Fig. 1, Rodriguez et al., 2009). Two-sigma conservative thresholds on the two area distributions are automatically calculated in order to select only pixels corresponding to clouds. Each selection is then visually checked and the thresholds are eventually tuned to assure that all detections are real and that we do miss as few "cloudy" pixels as possible. We still deliberately choose conservative thresholds to avoid false positives. This can lead to the non-detection of optically thin or very low clouds, of clouds that are much smaller than a VIMS pixel, or of clouds that are too close to the limb (see Table A1 from the Appendix).

Finally, once the "cloudy" pixels are selected by our algorithm within an image, they are reprojected on Titan's globe. This process is repeated for each of the 2000 selected VIMS datacubes spanning 2004–2010, to produce the final detection maps and time evolution plots. The reprojection of VIMS pixels on Titan's globe is the essential final step of our computations and is carried out by navigating the Cassini observations. The navigation is the mathematical process that assigns longitude and latitude coordinates to the four corners of each pixel on the image plane, as well as geometric information such as incidence, emergence and phase angles. We developed software that (1) calculates the rotation matrix of the VIMS focal-plane-based coordinate system to the planet-based coordinate system, (2) applies this rotation to all the image pixels, and (3) computes the intersection with the planet ellipsoid expressing the results in terms of longitude and latitude coordinates. Our navigation code uses functions of the ICY toolkit and ancillary data stored in SPICE kernels (Spacecraft Planet Instrument C-matrix Event) provided by the Navigation and Ancillary Information Facility (NAIF; http://www.naif.jpl.nasa.gov/naif/). This code was already successfully applied to VIMS images of Titan, for surface studies and cartography (Sotin et al., 2005; Rodriguez et al., 2006; Le Mouélic et al., 2008b; Le Corre et al., 2009), as well as for haze study and cloud tracking (Le Mouélic et al., 2008a; Rodriguez et al., 2009; Rannou et al., 2010).

This cloud mapping algorithm has been recently improved by introducing capabilities to (1) select regions of interest, (2) mask Titan's bright limb that often prevented the detection of the dimmest clouds, and (3) help the visual checking of the detections

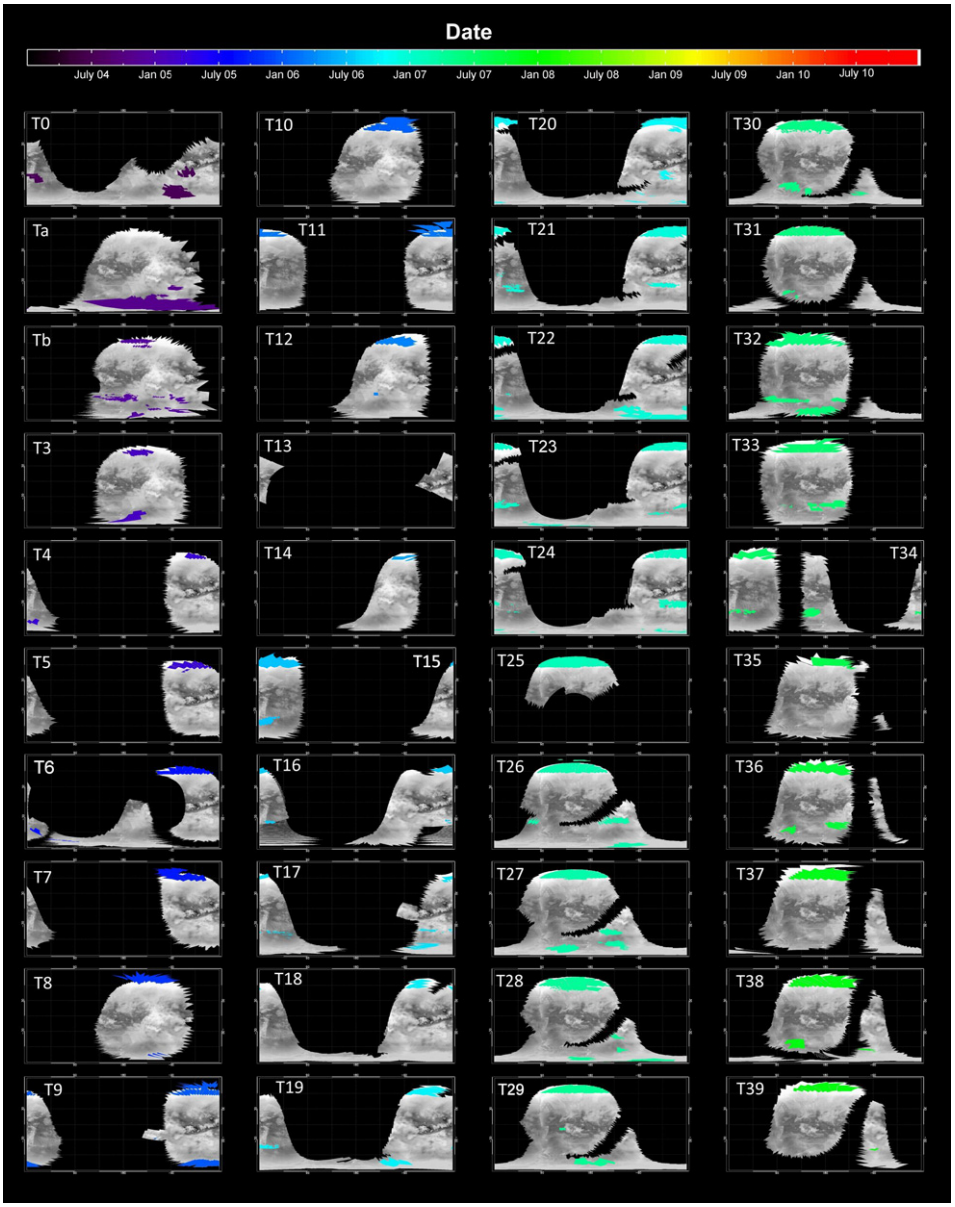

Fig. 1. Maps of clouds observed by VIMS onboard Cassini during each of the 67 Titan planned flybys from July 2004 (T0) until April 2010 (T67). The mapping projection is rectangular with grid marks every 45° of longitude and 30° of latitude (0° longitude is on the left). Longitude is in degrees east. A VIMS map of the observed areas is used as background for each flyby. The resolution of the projection maps are of 0.3° in longitude and latitude (~14 km per pixel at the equator). Cloud detections are marked on each map with a rainbow color coding corresponding to the period they were observed (the precise flyby dates are referenced in Table A1 of the Appendix).

using the 2.1 μm VIMS channel, which is sensitive to tropospheric clouds. All the cloud detection maps shown in this study were produced with this new version of the detection algorithm.

Brown et al. (2010) pursued an alternate approach by using pure visual cloud detection. See the Appendix for a detailed comparison of the two methods and their results.

3. Results

3.1. Global view of the 2004–2010 cloud coverage of Titan

Using the method described in Section 2, we select only cloud pixels within the whole VIMS dataset between July 2004 (Cassini flyby tagged T0) and April 2010 (T67). The selected pixels are gathered in time clusters corresponding to the duration of each individual Titan targeted-flyby and are then reprojected into the planetocentric Titan coordinate system to produce the 67 individual cloud detection maps shown in Fig. 1. These maps use as background a VIMS global mosaic with a mask corresponding to the dayside coverage recorded during the corresponding flybys. From T0 up to T38, the maps presented here correspond to updated versions of the one presented in Rodriguez et al. (2009). They comprise 20 new detections and include shape improvements for six previous detections (see the Appendix for details). The total of 220 clouds shown in our detection maps are all referenced and documented in Table A1 of the Appendix to allow further comparisons with other studies.

Fig. 2a summarizes both the data analyzed and the clouds detected during the 6-year period. The cumulative number of cloud observations between July 2004 and April 2010 is illustrated in Fig. 2b. It corresponds to the number of times that a cloud has been observed by the VIMS instrument at a given location. The cloud count varies from 0 to 30, with a mean value of 2. The total number of VIMS observations at a given point is mapped in Fig. 2c. This

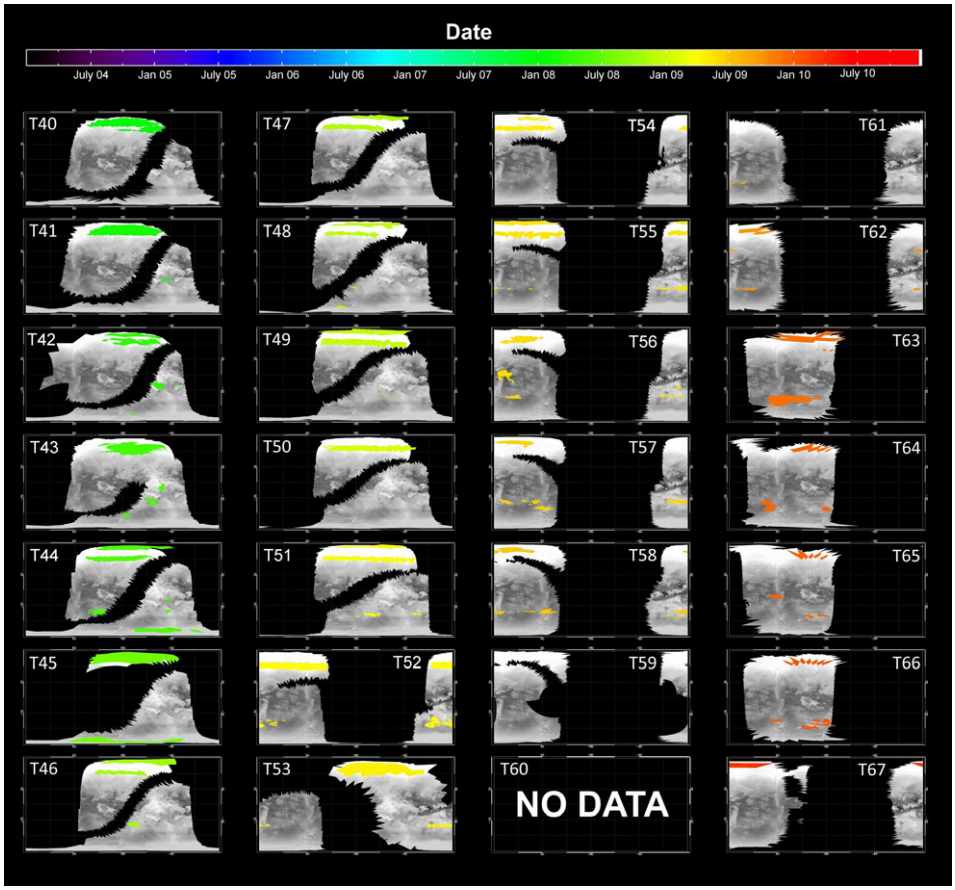

Fig. 1 (*continued*)

number varies between 1 and 53, with a mean number of 29. The fractional cloud coverage (Fig. 2d) is calculated by dividing the number of cloud occurrences at a given latitude/longitude location (Fig. 2b) by the number of VIMS observations of that location (Fig. 2c). This operation compensates for the systematic biases coming from the widely varying VIMS coverage. It is important to consider all of these maps together when drawing conclusions. For example, there seem to be less cloudy areas well localized in the northern polar region at ~90°E and −45°E longitudes (holes in the uniform north polar cloud blanket). These particular areas correlate, in fact, with a lower sampling. Indeed these particular regions were imaged only 0–10 times by VIMS, with very coarse spatial resolution (greater than 200 km per pixel) and often in limb viewing conditions; hence their identification as 'holes' is statistically insignificant. Elsewhere on Titan, the VIMS coverage is sufficient to consider the averaged fractional cloud coverage presented in Fig. 2d with higher confidence.

On a global scale, Titan's cloud coverage is very low relative to terrestrial standards, with a very patchy cloud coverage. Averaged over the period interval between July 2004 and April 2010, the cloud coverage only represents ~10% of Titan's entire globe. In comparison, the instantaneous cloud coverage on Earth is seven times greater (~75%) on average (Mace et al., 2009). Between northern winter and the beginning of spring (the 2004–2010 period), Titan's clouds have mostly occurred in three areas which are well delineated in latitude (Fig. 2d): (1) the north polar region, (2) the temperate southern latitudes, and (3) the south pole. Other regions are almost completely free of clouds, except for very sporadic tropical outbursts and two small clouds at northern mid-latitudes (~40°N).

3.2. Time evolution of Titan's cloud activity from 2004 (winter) up to 2010 (spring)

The seasonal evolution of the large-scale geographic distribution of clouds is a strong marker of the global atmospheric circulation on Titan (Tokano et al., 2001; Tokano, 2005; Rannou et al., 2006; Mitchell et al., 2006, 2009; Turtle et al., 2009; Rodriguez et al., 2009). We present in this section the time evolution of the main cloud structures that we identified in our observations. Fig. 3 shows the time evolution of the latitudinal distribution of Titan's clouds between July 2004 (winter) and April 2010 (spring) as seen complementarily by Earth-based telescopes (Roe et al., 2005b; Schaller et al., 2006b, 2009; de Pater et al., 2006; Hirtzig et al., 2006) and Cassini (Porco et al., 2005; Baines et al., 2005; Griffith et al., 2005, 2006; Le Mouélic et al., 2008a; Turtle et al., 2009; Rodriguez et al., 2009; and this study). Fig. 4 also presents the evolution of Titan's cloud cover during the same period, but provides additional information on the regional evolution of this distribution by showing maps of fractional cloud coverage over four time periods. This figure shows the global and latitudinal fractional cloud coverage for four periods from Cassini flyby T0 (1st of July 2004) up to T16 (22 July 2006), T17 (7 September 2006) up to T40 (5 January 2008), T41 (22 February 2008) up to T58 (8 July 2009), and T59 (24 July 2009) up to T67 (5 April 2010).

3.2.1. North polar cloud

The northern polar region of Titan is systematically blanketed by an ever-present thin cloud system from the first Cassini observations in mid-2004 until early 2008. As Titan's north pole progressively emerges from the night, this large, stratiform cloud system is

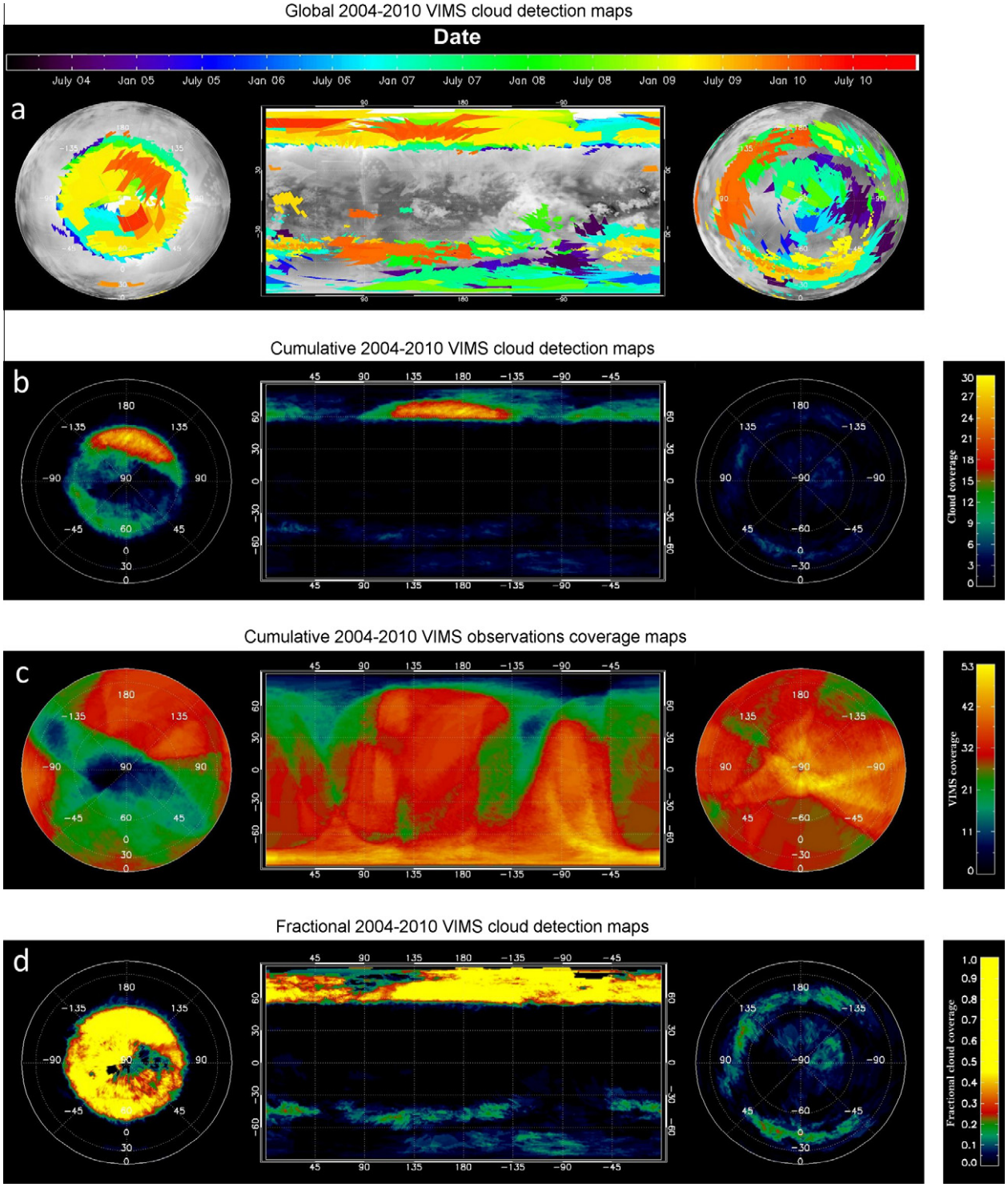

Fig. 2. (a) Synthesis of the cloud detections made by VIMS/Cassini between July 2004 and April 2010. The rectangular projection (middle), the basemap and the color coding are similar to those of Fig. 1. For the northern (left) and southern (right) polar projections, grid marks are shown every 45° of longitude and 30° of latitude (0° longitude is down). Longitude is in degrees east. (b) Cumulative number of clouds detected by VIMS in the 2004–2010 period. The color scale shows the number of times that a cloud was observed at each location. (c) Coverage of VIMS observations in the 2004–2010 period. The color scale shows the number of flybys during which each point of Titan was imaged by VIMS with an incidence angle lower than 90°. (d) Fractional cloud coverage in the 2004–2010 period is obtained by dividing (b) by (c). The color scale saturates at 0.45 to enhance the southern cloud distribution and equatorial transient events. The fractional coverage in clouds of the north polar region exceeds 0.7 almost everywhere poleward of 60°N. The clouds of Titan mainly cluster at three distinct latitudes during the course of southern summer and at the beginning of southern fall: poleward of 60°N, poleward of 60°S and at ~40°S. The resolution of all the rectangular and polar projections shown here are similar to those of Fig. 1 (0.3° corresponding to ~14 km per pixel at the equator).

found to cover the polar region at all longitudes and from ~60°N latitude up to the pole (Griffith et al., 2006; Le Mouélic et al., 2008a, 2011; Rodriguez et al., 2009). Poleward of ~60°N the fraction of cloud coverage, averaged over the 2004–2010 period, is greater than 70% (Fig. 2d). Its total surface coverage however has slightly diminished with time. Very stable between 2004 and 2006, with an overall fractional coverage greater than 80% (black curve in Fig. 4e), this large cloud started slowly recessing since

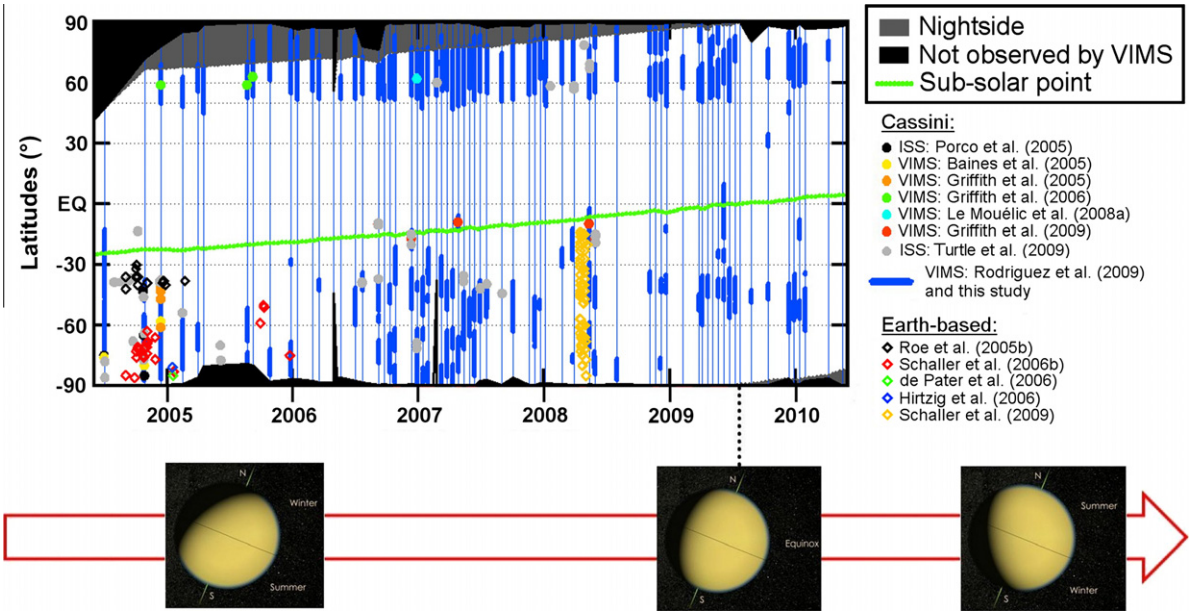

Fig. 3. The latitudinal coverage of Titan's cloud activity with time between July 2004 and April 2010. Each thin blue vertical solid line marks the time of Cassini flyby of Titan as well as the latitude coverage of the VIMS observations. The larger blue lines show the latitude extension of clouds that we detected with VIMS, summed over all longitudes. Our detections are in very good agreement with previous Cassini (colored dots) or Earth-based (colored diamonds) observations. The green line shows the latitude of the sub-solar point indicating the region of the maximum of solar insulation. Northern spring equinox occurred in August 2009. At that time, the solar maximum was at the equator. (Credits for the views of Titan seasonal illumination: © Animea, F. Durillon).

mid-2006 (blue curve in Fig. 4e). After mid-2008, the north polar cloud began to fractionate and collapse at some places, leaving a cloud ring centered at ~60°N with only small, but more opaque and convective-type cloud patches in its central region (Figs. 1, 3, 4c and green curve in Fig. 4e). Later on, as Titan passed the spring equinox in August 2009, all that had remained from the large north cloud cap, including the thin ~60°N cloud ring, finally disappeared, leaving the north pole free of cloud, apart from small and sporadic clouds (Figs. 1, 3, 4d and red curve in Fig. 4e), likely to be convective in nature. A detailed analysis of the Titan's north polar cloud seasonal recessing can be found in Le Mouélic et al. (2011).

3.2.2. South polar outbursts

Large clouds are also clearly visible at the south pole since the early VIMS observations of Titan in 2004 (Figs. 1, 3 and 4a). Cloud events at Titan's south pole have been previously reported from Earth-based observation campaigns since December 2001 (Brown et al., 2002; Roe et al., 2002; de Pater et al., 2006; Hirtzig et al., 2006; Schaller et al., 2006a, 2006b, 2009). From telescopic observations, these clouds appeared to be tropospheric large scale stormy outbursts with variability timescales (related to their changes in size and/or height) of a few hours (Schaller et al., 2006a). These storms have sustained their activity almost continuously until November 2004, from which time they were also observed by Cassini (Porco et al., 2005; Baines et al., 2005; Turtle et al., 2009; Rodriguez et al., 2009; this study). Contrary to what was previously thought from Earth-based imaging (Schaller et al., 2006b), south polar clouds have still retained a substantial activity after this date. They were indeed constantly detected by VIMS after November 2004 up to December 2005, during almost all Cassini flybys of Titan (Figs. 1 and 3). Nevertheless these events were dimmer and less spatially extended than those seen since 2002, possibly preventing Earth-based telescopes from resolving them. After December 2005, the cloud activity at the south pole began to decline. For the first time since 2001, no clouds near the south pole were observed for 8 months, between January and September 2006 (Figs. 1 and 3). Large outbursts were then regularly detected again for almost a year (Figs. 1, 3, 4b and c). Except for some rare and small scale events in 2008, the south pole of Titan ceased all stormy activity starting from the last dissipation in mid-2007, 2 years before the northern spring equinox (Figs. 1, 3, 4c and d). This decline is illustrated by the gradual decrease of the mean fractional coverage in clouds poleward of 60°S between 2004–2006 (~15%) and 2009–2010 (down to 0%) periods (black to red curve in Fig. 4e).

3.2.3. Southern mid-latitude clouds

On the other hand, southern mid-latitude clouds were observed by ISS (Turtle et al., 2009) and VIMS (Rodriguez et al., 2009; this study) on a regular basis between July 2004 and April 2010 (Figs. 1 and 3). Indeed, recent VIMS observations show that southern mid-latitudes (regions of Titan between 30°S and 60°S) showed a relatively stable fractional coverage in clouds of ~10% during the entire 2004–2010 time interval (Fig. 4a–e), reaching a peak mean fractional coverage of ~15% between July 2009 and April 2010. These clouds were thus still present, and quite active, at the time of the northern spring equinox (August 2009), and do not seem to display any sign of decline after that date thus far. Southern mid-latitude clouds are generally found to be elongated in the east–west direction, likely stretched by zonal wind shear at the altitude where they form (Griffith et al., 2005; Rodriguez et al., 2009).

3.2.4. Tropical and northern mid-latitude clouds

After December 2006, we identify some clouds further north in Titan's tropics, equatorward of ± 30° latitudes (green to reddish colors in Figs. 1 and 2a). Most of them are found in the southern hemisphere (Figs. 1, 2a and 3). Some of these clouds were also reported in other studies (Porco et al., 2005; Griffith et al., 2009; Turtle et al., 2009; Rodriguez et al., 2009; Schaller et al., 2009). However, contrary to what we observed in the high- to mid-latitude regions of the southern hemisphere, these near-equatorial clouds were in general much smaller (except for the T56 and T65 events) and significantly more scarce, appearing in less than ~5% of the 67 Cassini flybys between July 2004 and April 2010 (Figs. 2d and 4). Their scarcity is not due to a spatial resolution effect. Indeed, for example, the small

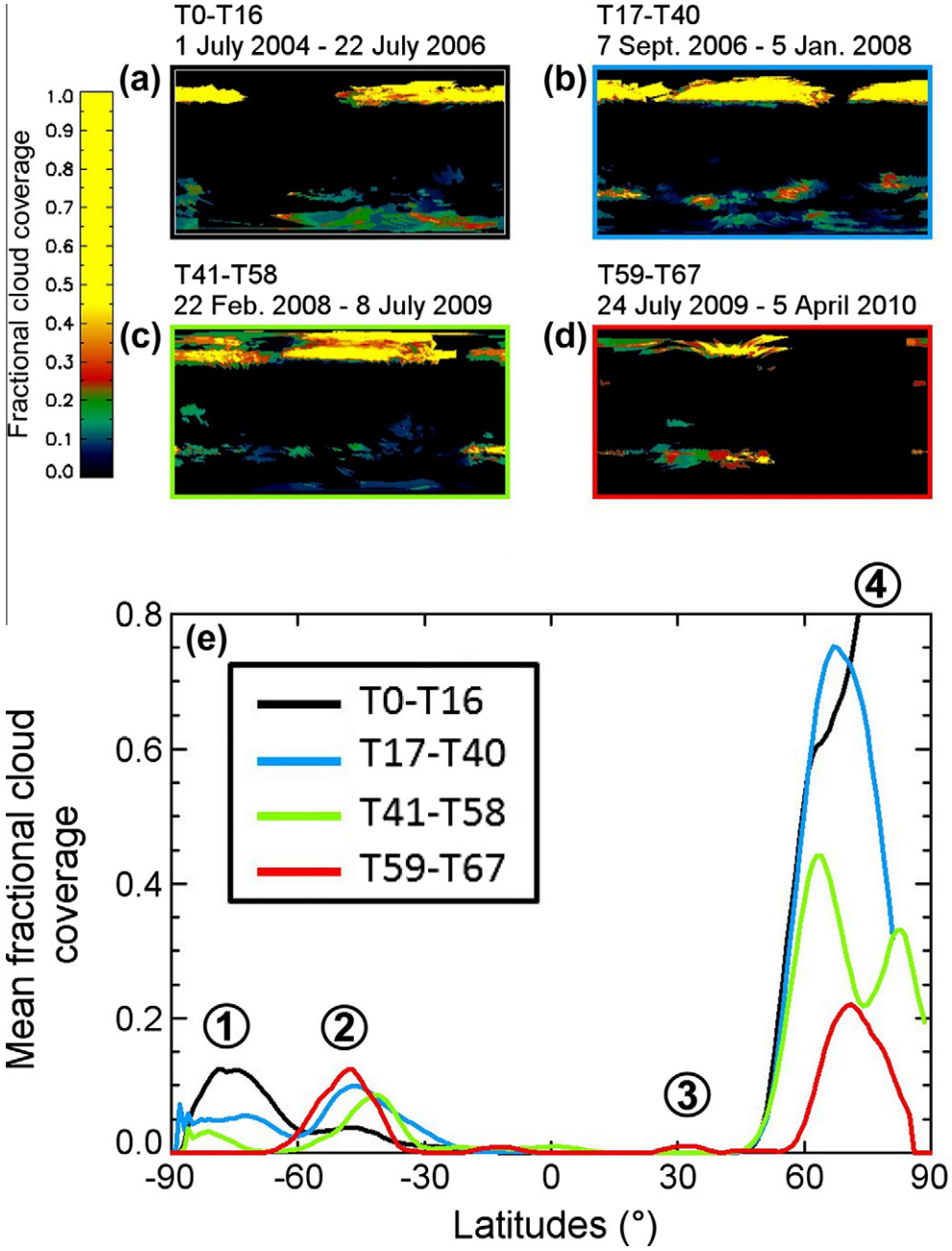

Fig. 4. (a–d) Maps of fractional cloud coverage on Titan for four successive periods (July 2004–July 2006, September 2006–January 2008, February 2008–July 2009, July 2009–April 2010), using the same conventions as in Fig. 1. The time resolution is slightly sharper for the last two periods as they are closer to the equinox. (e) The corresponding fractional cloud coverage as a function of latitude for the four periods considered in Fig. 4a–d. The latitudinal fractional cloud coverage curves are obtained by averaging the fractional cloud coverage maps (a–d) over longitudes. These distributions are all smoothed by a 10° boxcar smoothing. Encircled numbers indicate particular regions of interest: ① and ④, the south and north polar regions respectively, showing a drastic decline of cloud activity, ②, the southern mid-latitudes with a rather constant high activity (even after the equinox as shown by the red curve), and ③, the northern mid-latitudes with signs of very sporadic cloud activity beginning here around equinox.

tropical clouds observed during the T41 flyby (22 February 2008) were detected with a mean spatial resolution of 70 km/pixel, demonstrating the capability of VIMS to detect clouds with such a coarse resolution, with which more than 90% of Titan's surface has been imaged. Despite their sparsity, we notice that equatorial clouds appear with a slightly higher frequency after February 2008, during the approach of equinox.

Finally, we also observe the first, consecutive appearances of two small elongated clouds at northern mid-latitudes (flybys T62 and T63 in Figs. 1, 4e and 7). These unique clouds have an elongated morphology similar to the ~40°S clouds, and are not connected to the north polar cloud (orange color in Figs. 1 and 2a). They first appeared in late 2009, right after the northern spring equinox (Fig. 3 and red curve in Fig. 4e), and were observed while ~40°S clouds were still active.

4. Discussion

4.1. General circulation and Titan's climate: comparison with predictions of GCMs

The observation of Titan's cloud distribution and its evolution with season provides critical constraints on models of Titan's atmospheric circulation. Comparing the common features and

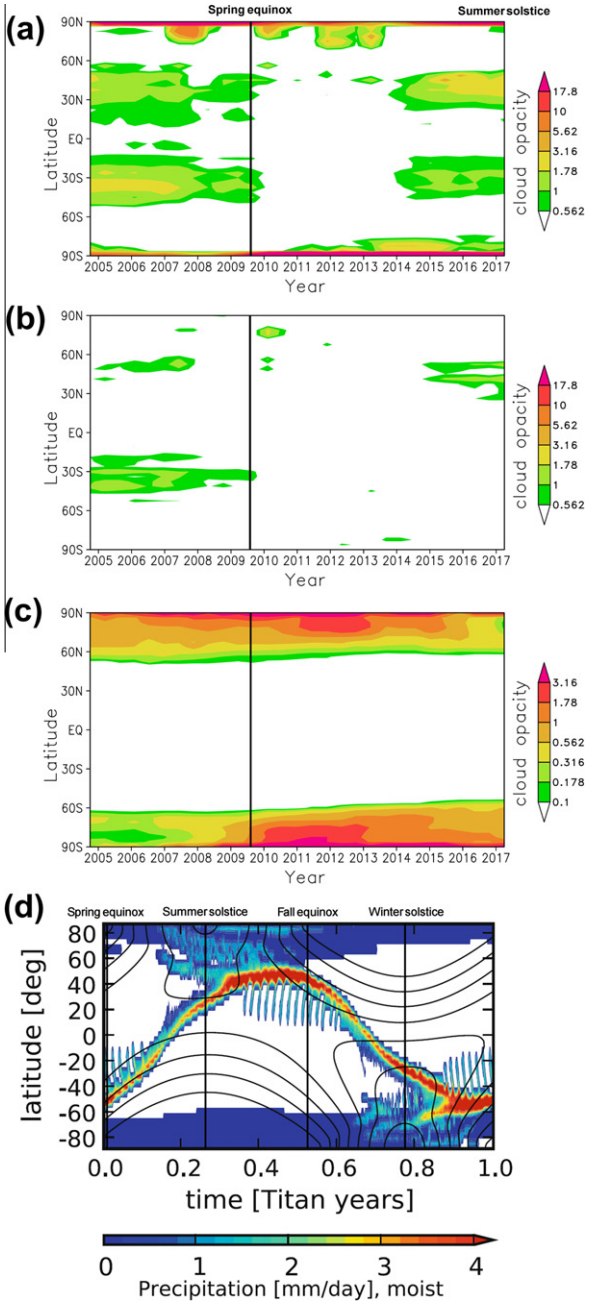

Fig. 5. (a–c) Maps of Titan's cloud opacity, averaged over five consecutive years, between the ground and the pressure level 400 mbar (~23 km altitude), showing the coverage of methane clouds (a) and ethane clouds (b), and above 400 mbar showing only the ethane clouds (c), as predicted by the atmospheric global circulation model of Rannou et al. (2006) (IPSL-TGCM), between 2004 and 2017. In these simulations, the methane condensates dominate the opacity below 400 mbar and the model shows that the large and sporadic cloud structures seen at mid-latitude and very near the poles are due to methane (a and b). On the other hand, the upper layer of cloud (c) is dominated near the poles by ethane condensate (with the north polar cloud thicker that the southern one in 2006). No methane cloud is produced above 400 mbar in these simulations. Although it remains less opaque that the low altitude methane cloud, the ethane cloud is best observed from orbit in the northern region because it is well above the methane condensation altitude. Note that these maps give the main structure of the cloud layer, but they are made from simulations which are not optimized to fit the most recent Cassini-Huygens observations. (d) Predictions of methane precipitations in Titan troposphere for an entire Titan's year from the Mitchell et al. (2009) GCM (directly taken from Fig. 6c of Mitchell et al. (2009)). The precipitation rate is averaged over 10-Titan-day. The black curves illustrate the pattern of solar forcing at the surface. Readers can refer to the text for a detailed comparison between our observations and the predictions of both GCMs.

the differences between observations and predictions can drive enhanced comprehension of the physical processes controlling Titan's general circulation. Among the GCMs available for Titan that incorporate moist processes (Tokano et al., 2001; Tokano, 2005; Rannou et al., 2006; Mitchell et al., 2006, 2009; Newman et al., 2008), we compare here two models that document in detail the seasonal evolution of clouds and/or precipitation (Rannou et al., 2006; Mitchell et al., 2006, 2009). Both are two-dimensional axisymmetric (altitude–latitude). Yet, the physical processes that drive the dynamics of Titan's atmosphere and the cloud formation differ markedly from one model to the other. The Mitchell et al. (2006, 2009) model (1) is tropospheric only, (2) does not include the haze, (3) omits horizontal mixing processes, and (4) enables methane condensation where and when its atmospheric saturation ratio exceeds unity through parameterized moist convection. The methane condensation 'instantly' triggers precipitation, unless underlying atmosphere is subsaturated. The IPSL-TGCM (for Institut Pierre-Simon Laplace – Titan's General Circulation Model; Rannou et al., 2006) (1) goes up to the mesosphere at ~500 km altitude and dynamically couples all the atmospheric layers, (2) accounts for horizontal diffusion (by eddy angular momentum transport due to barotropic instabilities), (3) does not include moist convection, but (4) calculates and couples the haze and cloud microphysics regarding nucleation, methane and ethane condensation, and sedimentation (see Lebonnois et al. (2009) for a detailed review of the IPSL-TGCM). The different physics used by the two models lead to radically distinct predictions for the tropospheric cloud/precipitation seasonality. An abrupt shift of the meteorology from the winter to the summer hemisphere, only interrupted by a quiescent period of 3–4 terrestrial years after the equinox, is forecast by the IPSL-TGCM. On the contrary, the Mitchell et al. (2009) model predicts a smooth, continuous migration of precipitation from one hemisphere to the other between solstices. The time evolutions of Titan's cloud/precipitation latitudinal coverage as predicted by the Mitchell et al. (2009) model and the IPSL-TGCM (Rannou et al., 2006) are compared in Fig. 5.

4.1.1. Cloud preferential latitudes during Titan's winter

In the summer hemisphere, both model predictions for the preferential latitudes of cloud/condensation are very similar and in satisfactory agreement with the latitudinal distribution of the main tropospheric cloud structures that are observed: the mid-latitude band and the polar outbursts. Both models predict methane clouds or condensation to form at mid-latitudes in the summer hemisphere (~40–60°), precisely as observed by ISS (Turtle et al., 2009) and VIMS (Rodriguez et al., 2009; this study). This region corresponds in the GCMs to the rising branch of the tropospheric Hadley cell (the equivalent of Earth's Intertropical Convergence Zone, ITCZ). Both GCMs also predict sporadic methane clouds and precipitation to occur in the summer polar region. The Mitchell et al. (2006, 2009) model suggests that these polar clouds are caused by a complex of polar vertical moist convection of methane-rich air cells (Hueso and Sanchez-Lavega, 2006; Barth and Rafkin, 2007) that occurs only at summer pole. Alternatively, Rannou et al. (2006) propose that the convection and condensation is triggered very close to the summer pole by the existence of a slantwise circulation cell, forced by the temperature gradient, which brings methane-rich air from lower latitudes to the higher and colder latitudes. The convective nature of the summer hemisphere events, as predicted by the models, is consistent with the morphology and the transience of the clouds observed in the southern hemisphere during summer (Brown et al., 2002; Porco et al., 2005; Schaller et al., 2006a, 2006b). However, the match in latitudes between the GCMs predictions for the summer hemisphere and the observations is less accurate in the polar region than in the mid-latitudes. Neither of the two models produces

significant cloud cover/condensation at 65–85°S where most of the numerous convective polar clouds are observed. Nevertheless, the gap in cloud activity between ~50° and 65°S is well predicted by both GCMs.

The IPSL-TGCM predicts methane clouds at mid-latitudes in the winter hemisphere. Less intense than in the summer hemisphere, cloud activity at northern mid-latitudes is nevertheless expected by the IPSL-TGCM throughout most of southern summer. We do not see any, though. Indeed, no clouds were detected before the equinox in the 0–50°N latitudes by ISS (Turtle et al., 2009) or by VIMS (Rodriguez et al., 2009; this study). In comparison, the Mitchell et al. (2006, 2009) model does not predict any methane condensation in the winter hemisphere. As stated in Rodriguez et al. (2009), the erroneous prediction of the ~40°N clouds by the IPSL-TGCM during the southern summer is a failure of the model. In the IPSL-TGCM, the winter ~40°N clouds are not associated with the general circulation, the rising branch of the tropospheric Hadley cell being locked at southern mid-latitudes. These clouds in the model are rather associated with latitudinal transport of methane by eddy diffusion, produced by inertial instabilities, through the equator-to-pole temperature gradient. This differs from clouds produced by ascending motions, as for instance at ~40°S in the summer hemisphere. Rodriguez et al. (2009) showed that the IPSL-TGCM overestimates the equator-to-pole temperature contrast in the winter hemisphere by a least a factor two relative to what was measured by the CIRS instrument onboard Cassini (Jennings et al., 2009). This could explain why, in consequence, the model overestimates the efficiency of methane condensation and cloud formation at ~40°N during southern summer.

On the other side, the IPSL-TGCM predicts the appearance and the observed latitude of the widespread winter polar cloud with high fidelity. This polar cloud system is assumed to be stable over the winter season resulting from the tropospheric cooling of descending stratospheric air (Rannou et al., 2006). The descending winter polar branch of the stratospheric circulation is expected to bring air cells enriched in ethane and aerosols down to an altitude of ~30–60 km near the tropopause where the ethane can condense, above the altitude of methane condensation, which is in very good agreement with the Cassini/VIMS "from above" observations of Titan's north polar region (Griffith et al., 2006; Le Mouélic et al., 2011). This pole-to-pole circulation supplies the winter polar vortex, poleward of ~60°N, in large-scale drizzle of small ethane-rich particles which may settle and eventually replenish ethane in the northern lakes. The underlying polar methane clouds, even if present and more opaque, may be hidden most of the time from Cassini view by the extensive overlying ethane cloud layer. Methane clouds at lower altitude would become more clearly visible only when the ethane cloud starts to thin out, fractionate and disappear. It is worth noting that the non-prediction of this cloud by Mitchell et al. (2006, 2009) is not a failure, since their model is only tropospheric and does not incorporate the ethane cycle.

4.1.2. The seasonal evolution of the cloud cover, from winter to spring

With the most recent resolved observations through and beyond the northern spring equinox reported in this study, we have the opportunity to make specific comparisons, not only about the cloud distribution in latitude, but also about its time evolution.

The progressive disappearance of the north polar cloud, as monitored by VIMS between 2006 and 2010, is predicted by the IPSL-TGCM with the correct timing (this study and Le Mouélic et al., 2011). According to the model, the recession of the winter polar cloud is a clear sign of the onset of the circulation turnover that affects the descending branch of the stratospheric cell in the winter polar region.

In the opposite hemisphere, summer high- and mid-latitude cloud activity persists much longer than predicted by the IPSL-TGCM during approach to Titan's equinox. As observed by VIMS, the entire summer hemisphere experiences a significant time lag in the seasonal evolution of the cloud cover. According to the model, the southern polar clouds should have entirely disappeared since mid-2005, whereas we still observe significant cloud activity in these regions until mid-2008. This time lag was already documented in Rodriguez et al. (2009). Nonetheless, the complete disappearance of the southern polar cloud after 2009 provides more evidence for the onset of the tropospheric circulation turnover, even if delayed. Our recent observations do not yet show the ~40°S cloud activity disappearing, as predicted by the IPSL-TGCM to occur starting in mid-2007, though it is still possible that this will occur following a larger time lag. Since clouds are directly linked to the general circulation, these differences indicate that the Hadley cell persists longer in reality than in the IPSL-TGCM. There are two possibilities. First the thermal inertia of the ground may be greater than assumed in the model, as was first postulated by Rodriguez et al. (2009). However this is not likely since the value that the IPSL-TGCM used (2000 J m^{-2} $s^{-1/2}$ K^{-1}) is already larger than the expected values for Titan (~500 J m^{-2} $s^{-1/2}$ K^{-1}, see Tokano, 2005). A second, more satisfying explanation for the persistence of convective activity in the summer hemisphere brings into play the strong interaction between the ground humidity and the atmosphere. Mitchell et al. (2009), which reproduced more faithfully the observed persistence of ~40°S clouds, also showed that they can produce a time lag in the seasonal occurrence of clouds up to 3–4 terrestrial years by adjusting the importance of methane latent heat effects (done by varying the surface boundary layer humidity). In comparison, in Rannou et al. (2006), the methane source is set with a simple evaporation law from an infinite surface reservoir. Other prescriptions of the methane source, with different geographical distribution of liquid methane, and a complete feedback with the precipitation rate and location, will be tested in the future with the IPSL-TGCM.

Not seen during the whole northern winter, clouds are detected for the first time with VIMS at ~40°N latitude on two occasions during the T62 (12 October 2009) and T63 flybys (12 December 2009), a few terrestrial months after equinox (Fig. 1 and details in Fig. 6). According to the GCMs (Rannou et al., 2006; Mitchell et al., 2006, 2009), the perennial appearance of these northern mid-latitude clouds should be the markers of the completion of the seasonal atmospheric circulation turnover at the end of Titan's spring (which should not occur before 2015–2017 – see Fig. 5). Although single events are always hazardous to interpret, we can nevertheless point out that such early springtime clouds are unlikely to be associated with an early hemispherical shift of the ITCZ to the north (which is predicted to occur during the equinoctial transition phase and to take 3–4 terrestrial years after the equinox to complete (Rannou et al., 2006; Mitchell et al., 2009)). As the Hadley cell present in a planetary atmosphere is directly produced by and strongly linked to the seasonal solar forcing, only one ascending branch is expected to occur at a given time. If these ~40°N clouds were related to a rising branch of the tropospheric Hadley cell, and therefore with the completion of the circulation turnover within the troposphere, we would not have observed the systematic coexistence of such events with persistent clouds at ~40°S (this latter being likely to be associated with the ITCZ still locked in the southern hemisphere at the end of southern summer and the very beginning of northern spring). It is thus impossible for the circulation turnover process to be at the same time delayed in the southern hemisphere and in advance in the northern hemisphere. However, the onset of the circulation turnover and the motion of solar insulation towards the north may modify the condition of latitudinal transport from the tropics towards the north pole (strengthening of the eddy diffusion) and may occasionally produce more clouds further north, where no large scale

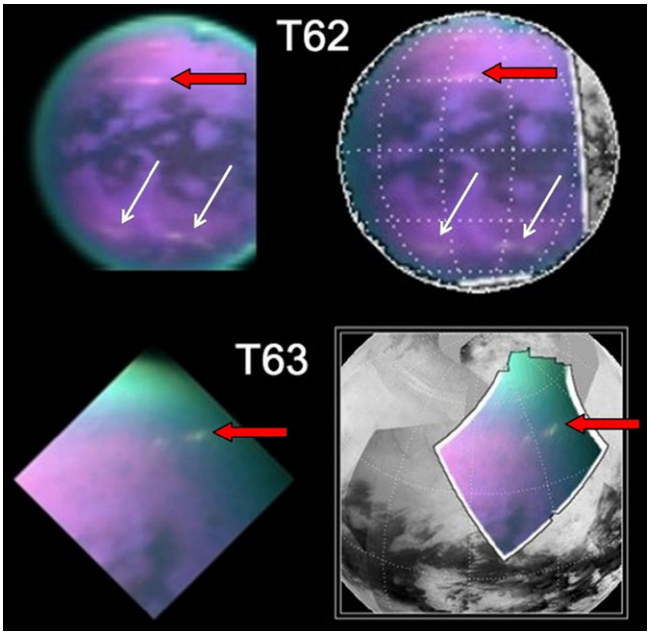

Fig. 6. First occurrences of northern mid-latitude clouds (red arrows) after Titan's equinox, at T62 (12 October 2009) and T63 flybys (12 December 2009). Raw (left) and orthographically reprojected VIMS images (right) are color composite using the 5-μm channel as red, the 1.6-μm as green and the 1.27-μm as blue. Clouds show up as bright elongated streaks. Southern mid-latitude clouds (white arrows) were still active at that time (see T62 – left).

upward motions are expected. GCMs generally predict large scale circulation and may miss local, but strong circulation able to produce ascending motion and clouds. If we consider that the ITCZ stays locked at summer mid-latitudes (Rannou et al., 2006), as suggested by the invariable observation of clouds at ~40°S, local scale circulations could explain the more frequent occurrence of clouds near the equator, as Titan is going through and beyond equinox and tropics are more and more powered by solar illumination. Another explanation is that such singular events may also be related to events totally external to climatology, such as strong degassing from the ground. Only the long-term monitoring of these latitudes will help to discriminate between these possibilities.

The combination of (1) the cessation of 'winter-type' cloud activity at both poles (convective clouds at the south pole and large ethane cloud cap at the north pole), (2) the constant appearance of clouds at 40°S through mid-2010, (3) the occurrence, a few months before and after the equinox, of more frequent equatorial clouds, and (4) the first appearance of northern mid-latitude clouds clearly indicates the onset of the circulation turnover and seems to imply an 'abrupt' hemispherical reversal of cloud activity, as predicted by the IPSL-TGCM, rather than a gradual migration of precipitation from the southern to the northern hemisphere (Mitchell et al., 2006, 2009). Nevertheless, as our monitoring in the present work ceases in April 2010, we still lack cloud observations after the equinox and the observation of Titan's meteorology during the entire equinoctial transition phase will be essential to understanding the real nature and timescale of the circulation turnover.

4.2. Longitudinal distributions of clouds

The only GCMs that predict and map the evolution of the cloud cover (Rannou et al., 2006) or methane precipitation (Mitchell et al., 2006, 2009) are only a 2D representation, in latitude and altitude. Therefore, they do not predict longitudinal variations in the cloud coverage. At the north pole, where ethane clouds are predominantly formed by downwelling, no longitudinal variations are expected. On the other hand, the clouds in the summer hemisphere are formed by upwelling which can be affected by surface properties such as topography, hydrocarbon sources (lakes, cryovolcanism) and temperature, and by wave propagation in the lower atmosphere. The observation of the distribution of clouds with longitude allows further exploration of the possible interaction between the general atmospheric circulation and processes that are related to the surface or to external forcing (e.g., Saturn's tides).

4.2.1. The south pole area during southern summer

Fig. 7 shows the fractional cloud coverage for the southern high latitudes for two successive periods: 2004–2007 and 2007–2010. Fig. 7d shows in particular the fractional cloud coverage as a function of longitudes averaged between 90°S and 60°S, for these two periods. Between 2004 and 2007, in the middle of southern summer, the south pole fractional cloud coverage presents significant variations with longitude (Fig. 7b and blue curve in Fig. 7d). At these latitudes and during that period, the cloud coverage was globally greater in the leading hemisphere (between −180°E and 0°) than in the trailing. This distribution clearly peaks at ~10% of fractional coverage at −120°E, 60°E eastward of Ontario Lacus (Fig. 7a), the largest lake of the southern high latitudes, with some spreading around the anti-Saturn point (180°E), just above the lake. The 2007–2010 period shows an obvious decline in cloud activity in the southern polar region, as summer ends and fall begins (Fig. 7c and red curve in Fig. 7d). Nevertheless, at that time as well, notable cloud coverage occurs only near Ontario Lacus and eastward of it. In contrast, the opposite side of Titan, around 90°E, shows few to no clouds throughout the observation period.

The curves of the fractional cloud coverage as function of longitude for the 2004–2007 and 2007–2010 periods have a very similar shape (Fig. 7d). At first order (large scale), it seems that one can go from one to the other by only applying a multiplicative factor. This implies that the processes governing the localization of south pole clouds in the leading hemisphere between 2004 and 2007 and between 2007 and 2010 must have a similar origin. A possible explanation is that Ontario Lacus, helped by the polar pattern of the general circulation (very active in the middle of the southern summer) and of the zonal winds, may act as a local catalyst for cloud formation and clustering (Brown et al., 2009; see Fig. 8). Ontario Lacus is the largest, and only stable lake filled with liquid hydrocarbons yet identified in Titan's south polar regions (Brown et al., 2008; Turtle et al., 2009). As methane, and ethane to a greater extent, has a very low evaporation rate under Titan's surface conditions (Mitri et al., 2007), Ontario Lacus is expected to evaporate only by a few meters and to be large and deep enough to persist over seasons, at least during the last few thousands of years (Aharonson et al., 2009; Wall et al., 2010; Hayes et al., 2010). During summer in the southern hemisphere, the local surface and near surface humidity would increase in the vicinity of this natural reservoir of liquid hydrocarbons with an efficiency higher than anywhere else in the south polar regions. At the same time, a small and oblique tropospheric circulation cell is expected to occur in the south polar regions (Rannou et al., 2006), with an ascending branch rising up to altitudes of 20–30 km above the pole. The interplay between the large-scale polar circulation cell and the presence of Ontario Lacus would bring upward the local excess of humidity to altitudes where it can condense and form clouds (see Tokano (2009) for a detailed study of the impact of lakes on winter/summer polar meteorology on Titan). Zonal winds at that epoch (southern summer) and these latitudes (between 90°S and 60°S) are predicted by GCMs to be almost null to slightly retrograde (westward) at very low altitude and globally prograde (eastward) above 10 km with a wind speed of ~1 m/s (Tokano and

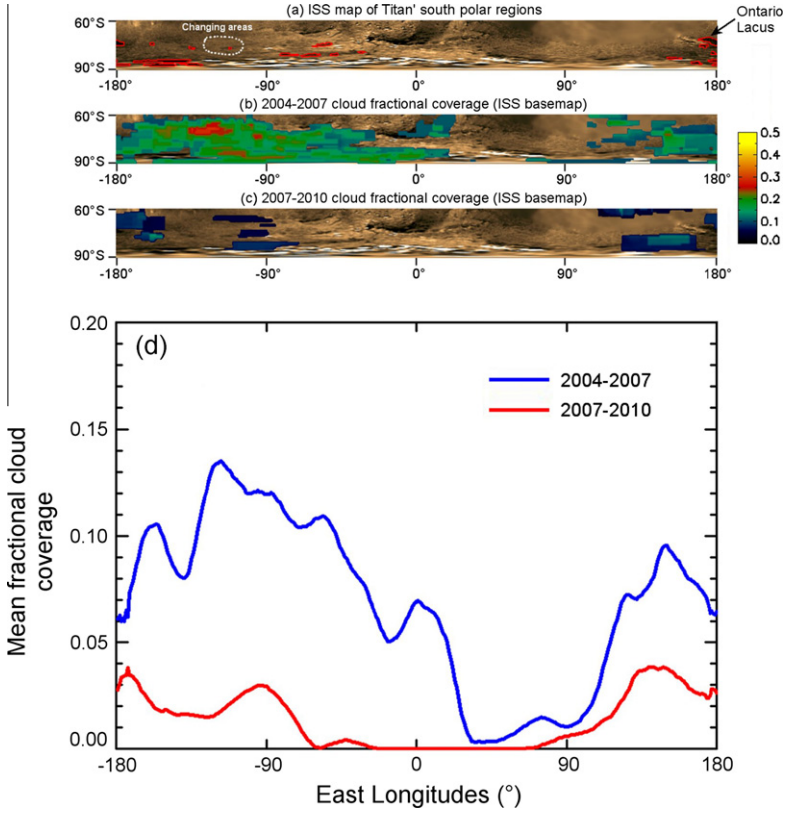

Fig. 7. (a) ISS rectangular map of Titan's southern region between 60°S and 90°S (colored from the grayscale map available at http://www.ciclops.org/). Ontario Lacus, centered at 180°E and 70°S, as well as other small areas potentially filled with liquids (as identified by Turtle et al., 2009) are outlined in red. The region where Turtle et al. (2009) identified evidences of surface darkening between 2004 and 2005 is outlined with the white dotted line. (b) Same ISS map of Titan overlapped by the 2004–2007 (from T0 up to T30 flyby) cloud fractional coverage. (c) ISS map of Titan overlapped by the 2007–2010 (from T31 up to T67 flyby) cloud fractional coverage. (d) Fractional cloud coverage as a function of longitudes, averaged between 60°S and 90°S, for the 2004–2007 (blue curve) and 2007–2010 (red curve) periods. These distributions are both smoothed by a 15° boxcar smoothing.

Neubauer, 2005; Rannou et al., 2006). That prediction is consistent with prograde wind speeds of a few meters per second retrieved at these latitudes from cloud tracking (Porco et al., 2005). These eastward winds would continuously push to the east these methane-rich rising air parcels, resulting in clouds preferentially formed eastward of Ontario Lacus. This effect is limited by the time scale of polar methane clouds sedimentation and lifetime, which is of the order of a few hours to a few days (Rannou et al., 2006). These clouds could be therefore transported eastward by this mechanism from 50 km up to 300 km before rainout occurs, which corresponds at these latitudes to 30–180° of possible longitudinal excursion east of Ontario. This scenario, also supported by the calculations of Tokano (2009), is fully consistent with the distribution of clouds observed by VIMS (Fig. 7b). The predicted zonal winds are only an average value and it is possible that some clouds could also, but more rarely, stay stationary above Ontario or reach regions slightly

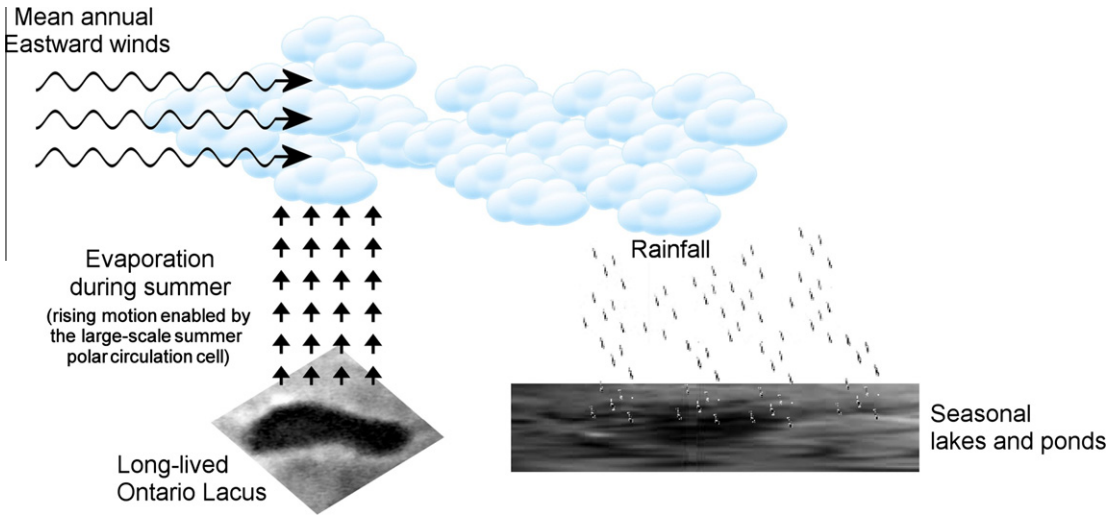

Fig. 8. Possible scenario invoking a local methane cycle and zonal winds occurring at southern high latitudes during the summer season. This scenario could explain the preferential distribution of clouds eastward of Ontario Lacus (see Fig. 7) and the surface changes reported by the ISS instrument between 2004 and 2005 (Turtle et al., 2009).

westward of it, as is also observed by VIMS (Fig. 7b). ISS images of the south polar regions showed that convective clouds and changes in surface brightness occurred between 2004 and 2005 (Turtle et al., 2009) at the place where VIMS observed the maximum of the south pole cloud distribution (see Figs. 7a and 6b). Indeed at ∼−120°E longitude and in the 70–80°S latitude range, ISS reported recent darkenings of the surface attributed to sporadic apparitions of liquid-filled depressions or ponds due to local and seasonal meteorology, in very good agreement with our scenario. The intensity of these processes must therefore be modulated by the general decline of southern cloud activity during seasonal change, when solar insolation energy flux diminishes, as it is indeed observed by VIMS (Fig. 7c).

4.2.2. Tidal control

We conducted a similar study of the cloud coverage distribution with longitudes for the mid-latitudes of Titan. Fig. 9 shows the fractional cloud coverage for the southern mid-latitudes for the same two successive periods of Fig. 7: 2004–2007 (dead of southern summer) and 2007–2010 (end of southern summer and beginning of southern fall). The fractional cloud coverage as a function of longitude, averaged between 35° and 55°S, is presented in Fig. 9d, for these two periods and an additional previous period of observations (2003–2005) obtained by an Earth-based campaign (Roe et al., 2005b). There is only a 6-month overlap between the Roe et al. (2005b) study and our first group of observations. As stated in Roe et al. (2005b) and Rodriguez et al. (2009), we observe significant longitudinal structures within the mid-latitude cloud distribution throughout the period between 2003 and 2010. After equinox, Titan's meteorology remained active at mid-latitudes (see Section 3.2). The distribution of cloud coverage with longitude shows a prominent peak of cloud activity roughly centered on the region facing Saturn ($0^{\circ}{}^{+30^{\circ}}_{-10^{\circ}}$ of east longitudes). This region never dropped below 18% in cloud fractional coverage, reaching 25% during the 2007–2010 period. A secondary peak about a third lower in intensity seems to emerge near the opposite side of Titan at ∼180°E (near the centre of the anti-Saturn hemisphere). Elsewhere, the fractional coverage never exceeded 10% on average during this time interval. We have now sufficient statistics in time coverage and number of cloud detections to consider that both of the peaks we observe with VIMS are real. However, it is possible that the displacement of the main peak of about 30° eastward between 2003–2005 and 2004–2007 reported by Rodriguez et al. (2009) was only due to statistical effects, as we observe now that 3 years later it returned, with no satisfactory explanation, to its early position reported in 2003–2005 by Roe et al. (2005b). The fact remains that the $n = 2$-mode wave pattern of the mid-latitude longitudinal cloud distribution, still present in 2010, as well as the loose correlation of the peaks of this distribution with any remarkable surface features, plead for an atmospheric origin for the cloud structuring in longitude. As proposed by Rodriguez et al. (2009), the sub- and, at a lesser extent, anti-Saturn bumps strongly suggest an external forcing by Saturn's tides. This mechanism, already suspected to generate strong and sudden changes in zonal winds patterns at some preferential longitudes 180° apart, due to interaction with perturbed vertical winds (Tokano and Neubauer, 2002), could also act to enhance or inhibit cloud formation in these locations. This hypothesis still needs to be tested by GCMs for Titan which include 3D atmospheric structure and wind dynamics.

4.2.3. Special case of Xanadu

Apart from its wavy pattern, one of the most striking structures of the longitudinal distribution of mid-latitude clouds is the very

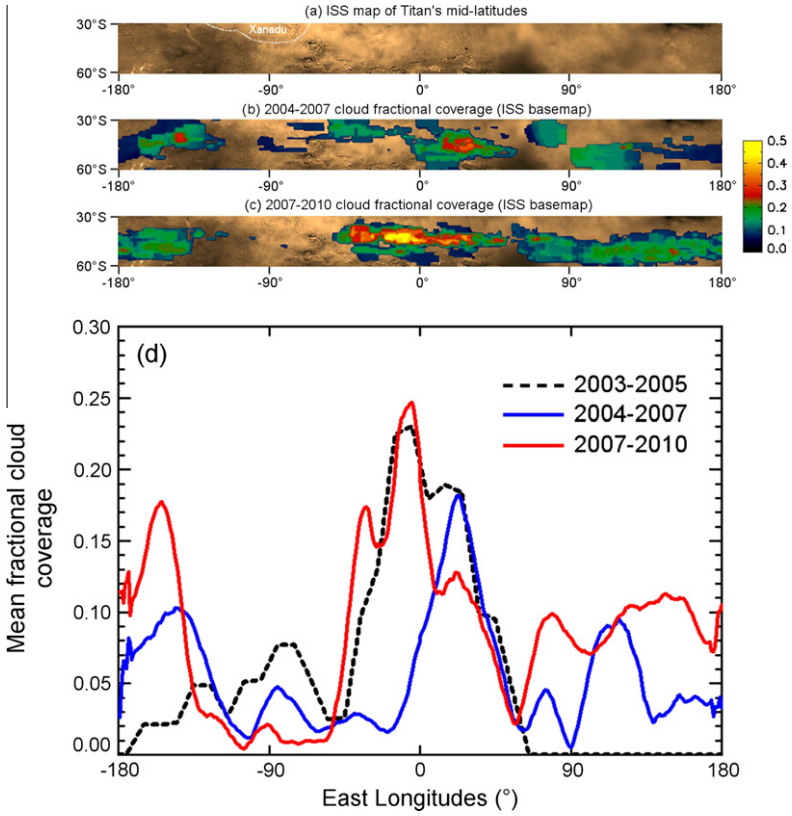

Fig. 9. (a) ISS rectangular map of Titan's mid-latitudes between 30°S and 60°S (colored from the grayscale map available at http://www.ciclops.org/). The southern part of Xanadu is outlined with the white dotted line. (b) Same ISS map of Titan overlapped by the 2004–2007 (from T0 up to T30 flyby) cloud fractional coverage. (c) ISS map of Titan overlapped by the 2007–2010 (from T31 up to T67 flyby) cloud fractional coverage. (d) Fractional cloud coverage as a function of longitudes, averaged between 35°S and 55°S, for the 2004–2007 (blue curve) and 2007–2010 (red curve) periods. These distributions are both smoothed by a 15° boxcar smoothing. The distribution reported by Roe et al. (2005b) from telescopic observations between 2003 and 2005 is also shown in black dashed line.

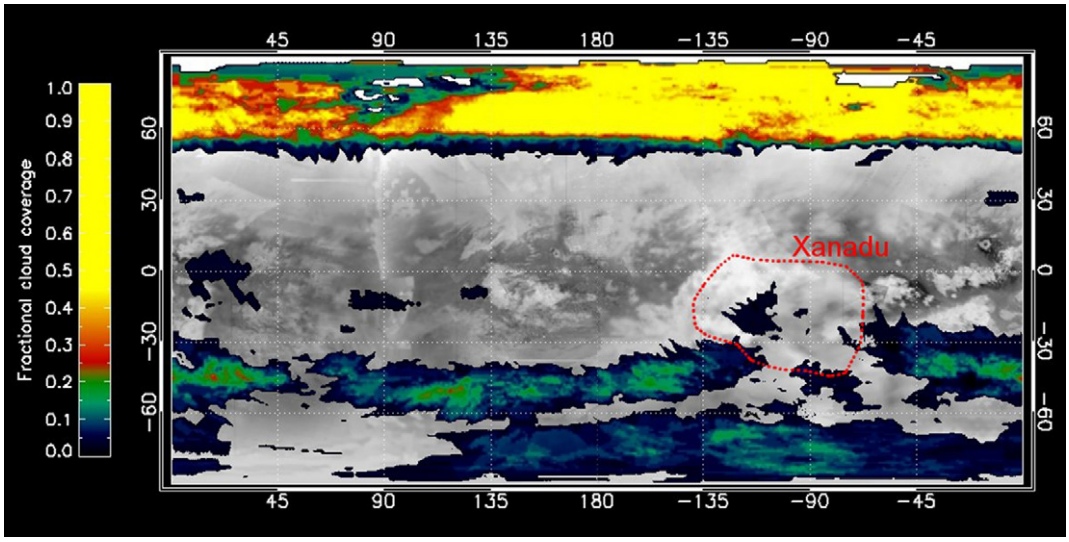

Fig. 10. 2004–2010 fractional cloud coverage map overlapping the VIMS map of Titan (similar to the one used in Figs. 1 and 2a). The Xanadu region is outlined with a dotted red line. The southern part of Xanadu shows clear evidences of cloud deficiency in comparison with the other regions at ~40°S regularly covered by clouds.

low cloud fractional coverage, below 5% on average, regularly found in the vicinity of −90°E longitude between 2003 and 2010 (see Fig. 9b, c, and curves of the Fig. 9d), interrupting the continuity of the mid-latitude cloud belt (see the global map of Titan in Fig. 10). This region of very poor cloud activity, ~50° wide in longitudes, lies right above the southern part of the peculiar Titan surface feature called Xanadu (see Figs. 9a and 10). Contrary to what was previously proposed (Adamkovics et al., 2007, 2009), we do not see any evidence in our data for an enhancement of methane condensation, precipitation or drizzle over Xanadu. Our long-term observations show that Xanadu seems to act more as an "obstacle" to cloud formation than a privileged area for condensation. Preferential condensation of methane right above Xanadu was previously contested by Kim et al. (2008) arguing that the Adamkovics et al. (2007) analysis was biased by surface artifacts.

In many respects, Xanadu is one of the most remarkable regions of Titan. Even from Earth-based telescopic observations, Xanadu is known to be among the brightest areas of the moon in the near-infrared, in the 0.93–2 μm range (Lemmon et al., 1993; Smith et al., 1996; Gibbard et al., 1999; Coustenis et al., 2001). The Cassini RADAR images of Xanadu revealed that most of the ~5 million km^2 area is dominated by extended mountain ranges that are thought to originate from Titan's large scale tectonism (Radebaugh et al., 2007, 2011). The uniqueness of this region is also noticeable from the Cassini RADAR radiometry experiment (Janssen et al., 2009). This is the only region of Titan to have such a combination of low emissivity, low dielectric constant (almost unity) and high volume scattering at 2.2-cm wavelength. It was interpreted as an area whose surface is globally covered by fractured ice largely overlain by a fluffy material. Long thought to be an elevated continent, recent altimetry investigations showed however that Xanadu is rather a large smooth depression, ~1 km deeper than the average geoid (Zebker et al., 2009).

Albedo and topography may significantly impact the atmospheric circulation and local meteorology. The effects of surface brightness and large-scale topography were examined by Tokano (2008) with the Cologne 3D GCM for Titan. They showed that the presence of Xanadu may markedly perturb the regional patterns of near-surface winds. In particular, if Xanadu is a large basin with a relative high albedo, they predict that the wind should then arc clockwise north of Xanadu and anti-clockwise west and south of Xanadu, in agreement with the dune orientations in the area. According to this model, incoming westerlies are ejected outside of Xanadu and become stronger and more unidirectional than inside Xanadu, leaving Xanadu's inside wind more erratic and quieter. It is possible that such large-scale near-surface wind perturbations generated by Xanadu may also impact the regional transport of humidity. The strong surrounding winds may cast the local humidity outside the boundaries of Xanadu, and therefore dry up the air inside regions of Xanadu and somewhat inhibit the cloud formation in this region. An alternative or complementary mechanism may be also invoked. If we consider again that Xanadu is a depression (Zebker et al., 2009), then the air that enters Xanadu and flows downward its slopes would adiabatically warm, contributing to the reduction of its relative humidity and suppressing cloud formation. These mechanisms need to be investigated by GCMs which include 3D atmospheric and cloud structure, wind dynamics and topography.

5. Conclusions

We have presented here the complete monitoring of cloud activity in Titan's atmosphere between July 2004 and April 2010, as observed by the VIMS instrument onboard the Cassini spacecraft. This 6-year long period covers northern winter up to early northern spring, including the equinox in August 2009. We developed a semi-automated algorithm to detect cloud contribution within the VIMS dataset and produced maps of the cloud coverage for each of the Cassini flybys of Titan, and derived the latitudinal and longitudinal distributions of the clouds and their evolution with time. The persistence, location, and periodicity of the clouds were compared with the forecast of the global circulation models (GCMs) (Rannou et al., 2006; Mitchell et al., 2006, 2009). These new constraints, along with ground-based observations, can contribute to the refinements of GCMs predictions and to a better understanding of Titan's climate.

Between 2004 and 2008 (i.e., late northern winter), we show that Titan's meteorology was very stable: (1) a widespread and long-lived cloud capped the entire northern polar vortex region, poleward of 60°N; apart from the polar cloud, the northern hemisphere (winter hemisphere) was entirely cloud-free and (2) sporadic clouds were regularly seen at mid-latitudes and above the pole in the southern hemisphere (summer hemisphere). Our observations support the interpretation that the winter (northern) polar cloud is caused by the sinking and cooling of stratospheric air into

the colder troposphere and the preferential condensation of droplets of ethane, and that the summer (southern) stormy clouds are more likely convective in nature and mainly composed of methane droplets. The latitudinal clustering of the clouds and the hemispheric asymmetry of their physical and chemical properties are both satisfactorily predicted by the GCMs.

After mid-2008, we observed the first strong evidence of a global decline of Titan's cloud activity. At the end of 2008, the clouds at the south pole disappeared. At the same time, the northern polar cloud began to show clear signs of fragmenting, finally to completely vanish after the equinox as predicted by the IPSL-TGCM (Rannou et al., 2006). We also detected a dozen cloud outbursts at the tropics, which seemed to be more frequent as equinox approaches. All these observations show that we are likely witnessing the onset of the seasonal pole-to-pole circulation turnover on Titan. The meteorology is then expected to completely reverse from one hemisphere to another in the next five or six terrestrial years, as predicted by the models. The persistence of southern mid-latitude clouds at 40°S through mid-2010, and the occurrence, a few months before and after the equinox, of more frequent equatorial clouds along with first appearance of northern mid-latitude clouds seem to suggest rather an abrupt hemispherical reversal of cloud activity, even if these equatorial and northern mid-latitude events are still too rare to be fully significant. The Cassini Solstice Mission will observe Titan up to the beginning of northern summer, in 2017, and should help to definitively solve the question of the meteorological hemispheric reversal, and the question of the type of atmospheric circulation (symmetric or asymmetric).

We also analyzed the longitudinal distribution of southern clouds at the time they were active. We found a prominent structure in the longitudinal distribution of clouds at southern high-latitudes that can be attributed to the presence of Ontario Lacus, the largest hydrocarbon reservoir in the region. As well, we observed that the southern mid-latitude clouds are distributed with an $n = 2$-mode wave pattern with peaks at 0° and ~180°E longitudes. Very stable with time, this pattern is interpreted to originate from Saturn's tides. In addition, we noticed a constant deficit of clouds at ~40°S and ~90°E, southward of Xanadu, which could be related to the local perturbation of winds and cloud formation by the large scale topography and high albedo of the Xanadu continent.

Areas significantly covered by clouds could also be interesting to observe as primary targets with imaging systems (radar and optical instruments) in order to detect surface features possibly related to rainfall events, or release of methane by subsurface processes or cryovolcanic activity. Continuing observations during the Cassini Solstice Mission will provide opportunities to investigate such phenomena.

Finally, our observation show that two-dimensional geometry for the GCMs must be extended to a fully three-dimensional grid in order to fully apprehend the impact of highly non-axisymmetric mechanisms on circulation and tropospheric cloud formation, such as the diurnal cycle of Saturn's tides or the topography. A fully 3D model may be also required to predict with more efficiency the haze and cloud microphysics and the seasonality of Titan's clouds and/or precipitation.

Acknowledgments

This work benefited from financial support from the Centre National de la Recherche Scientifique, Institut National des Sciences de l'Univers, from the French Centre National d'Etudes Spatiales (CNES) and from the ANR (project Exoclimat). Part of this work was performed at the Jet Propulsion Laboratory, California Institute of Technology, under contract to the National Aeronautics and Space Administration. We gratefully acknowledge the long years of work done by the entire Cassini and VIMS teams that allowed (and still allow) the acquisition of these outstanding sets of data. We also thank the two anonymous reviewers for very insightful comments and suggestions that helped the manuscript.

Appendix A. Comparison between Rodriguez et al. (2009) and Brown et al. (2010) Titan's clouds surveys

Brown et al. (2010) also analyzed the VIMS dataset with the same objective as Rodriguez et al. (2009) to map Titan's cloud occurrences during the Cassini prime mission. Brown et al. (2010) study extended the monitoring of Titan's clouds up to July 2008. Significant discrepancies with the study of Rodriguez et al. (2009) were pointed out.

For every ~9000 spectro-images of the nominal mission VIMS dataset, Brown et al. (2010) construct a set of three synthetic images referenced in their work as the "surface", "troposphere" and "stratosphere" images by combining VIMS channels only sensitive to Titan's surface, tropospheric and stratospheric features respectively. Each of the ~9000 triplets of images is visually inspected to search for clouds that appear in the surface and troposphere images but not in the stratosphere image. Finally for each of the images identified as having clouds, they hand-select all image pixels that contain a cloud, making a map of observed clouds on Titan for each image.

Table A1 presents the synthesis of each cloud detected in the VIMS dataset between July 2004 and July 2008 (Brown et al., 2010), July 2004 and December 2007 (Rodriguez et al., 2009) and January 2008 and April 2010 (this work). The location and the condition of observation of these cloud events is specified each time they are available. During the nominal mission, by merging all the studies from July 2004 to July 2008, a total of 163 individual cloud systems have been detected.

All these detections have been thoroughly reexamined by reanalyzing the entire VIMS dataset between July 2004 and July 2008. The fact is that any cloud detection technique has limitations because most of the time there is a continuum of I/F values rather than a clear separation between surface and cloud spectra. However, in order to be as accurate and objective as possible, we decide to conduct this reexamination by jointly taking advantage of the semi-automated source separation method (Rodriguez et al., 2009) and the use of the pure visual inspection of relevant VIMS channels (Brown et al. (2010). We thus performed a systematic re-analysis of each individual VIMS image by using simultaneously the 'objectivity' of the source separation technique and the 'sensitivity' of the tropospheric filter defined in Brown et al. (2010): cloud detection is ruled out if nothing is visible in the single 2.1 μm band and in the tropospheric filter, and if at the same time no specific feature can be isolated in the 2D scatterplot of the 2.75 versus 5-μm window integrated areas; on the contrary, if any feature shows up in the 2.1 band or tropospheric filter, or if the corresponding 2D scatterplot shows pixels isolated from the rest in the 2.75 and 5-μm high-value regions, the VIMS image is carefully considered and the feature is geographically isolated and thoroughly examined for cloud detection. A double independent and blind visual cross-checking of each new detection map thus produced, is then perform to further minimize the subjectivity and decide as firmly as possible between a robust detection and a rejection.

This detailed reexamination of the complete VIMS dataset shows that Rodriguez et al. (2009) missed 20 confirmed clouds (12.3% of total), have shape problems with 6 clouds (3.7% of total) and uncertainly detect 5 clouds (3.1% of total). More than 93% of the 143 Rodriguez et al. (2009) detections are therefore confirmed in terms of shape and location. The main drawback of the semi-automated routine of Rodriguez et al. (2009) is its lack of sensitivity in detecting the faintest clouds. This difficulty was previously

Table A1
Summary of Titan's clouds detected in the complete VIMS dataset between July 2004 and April 2010, classified by flyby and date (see also Table 1 in Barnes et al. (2009)). For each detections, when available, we indicate the central location of the cloud (in latitudes and eastern longitudes) and the conditions of observation (mean incidence, emission, phase and spatial resolution). The complete cloud characteristics are provided for Rodriguez et al. (2009) detections for the T0–T38 time interval (detection maps are available in Rodriguez et al. (2009) Supplementary Information: http://www.nature.com/nature/journal/v459/n7247/suppinfo/nature08014.html), fulfilled by this study up to T67. For T0–T44 time period, the cloud locations are completed with, and compared to, detections of Brown et al. (2010) (see Fig. 4 of Brown et al., 2010).

Sequence, Flyby # and date	Cloud type[a]	Avg. central lat. (°)	Avg. central East long. (°)	Mean inc. (°)	Mean em. (°)	Mean phase (°)	Avg. res. (km)	Notes [R09: Rodriguez et al., 2009] [B10: Brown et al., 2010]
S02/T0 (1 July 2004)	SP	−66	−80	44.5	42.4	60.7	88	One small patch, not centered above the SP
								Detected right above the SP by B10 with an extension not seen in the data
	TROP	−24	−64	6.6	77.4	76.1	88	Faint
								Detected by B10 10° higher in latitudes and with a more elongated, better shape than that in R09
	~40°S	−35	20	N/A				Very faint
								Not detected by R09
S05/TA (26 October 2004)	SP	−90		56.3	67	14.7	140	
	~40°S	−56	−107	48.3	61.7	13.9	116	
	~40°S	−46	−92	53.7	67.6	14	78	
S06/TB (13 December 2004)	SP	−80	−150	61	75.6	15.7	47	Large patch very near SP
								Detected by B10 with a better shape than R09
	~40°S	−50	157	46.6	56.4	15.3	56	Thin and elongated E–W
								Detected by B10 as a large patch too extended in latitudes
	~40°S	−43	−167	24.3	39.4	17.9	20	
	~40°S	−49	−77	43.7	54.4	15.4	52	
	~40°S	−50	−130	N/A				Very faint
								Not detected by R09
	~40°S	−31	−130	N/A				Not seen in the data
								Detected by B10 almost above the very bright Tui Regio
	NP	60	All	82.7	69.9	14.3	34	
S08/T3 (15 February 2005)	SP	−75	−145	N/A				Faint
								Not detected by R09
	NP	56	All	78.5	59.8	19.1	85.5	
S09/T4 (31 March 2005)	SP	−65	15	68.1	70.3	57	38	Very near the limb
								Not detected by B10
	SP	−70	−48	53.2	77.3	57.3	38	False detection by R09
	~40°S	−40	−42	N/A				Not seen in the data
								Detected by B10 as a very small streak
	NP	59	All	83.8	63.6	56.5	35	
S10/T5 (16 April 2005)	NP	45	All	67.4	53.5	55.5	74	R09 detect NP cloud at uncertain latitudes (too low)
S13/T6	SP	−67	90	N/A				Faint streak very near the terminator
								Not detected by R09
	~40°S	−58	20	N/A				Very faint
								Not detected by R09
	NP	59	All	N/A				Not detected by R09
S14/T7 (7 September 2005)	NP	72	All	94.4	81.3	51.5	62	
S15/T8 (28 October 2005)	SP	−75	−130	56.3	78.6	24.8	54	
	NP	73	All	95.3	78.4	22.6	75	
S17/T9 (26 December 2005)	SP	−76	45	60.4	79.4	28.5	83	
	TROP	−28	−119	66.9	71	137.9	9.8	Small cloud detected above Tui Regio at high phase angle
								Not detected by B10
	NP	73	All	94.7	77.1	26.6	70.5	
S17/T10 (15 January 2006)	NP	62	All	85.7	79.5	35.3	69	
S18/T11 (27 February 2006)	NP	75	All	98.2	81.2	17.3	93	
S19/T12 (18 March 2006)	~40°S	−38	−140	N/A				Extremely faint
								Not detected by R09
	NP	58	−73	75.9	78.3	63.2	142	
S20/T13 (30 April 2006)								
S20/T14 (20 May 2006)	NP	57	−90	76.4	80.2	91.2	106	
S21/T15 (2 July 2006)	~40°S	−45	25	N/A				Extremely faint elongated streaks
								Not detected by R09
								Detected by B10 as a huge complex. Haze artifact?
	NP	62	60	79	79.9	61	107	

Table A1 (*continued*)

Sequence, Flyby # and date	Cloud type[a]	Avg. central lat. (°)	Avg. central East long. (°)	Mean inc. (°)	Mean em. (°)	Mean phase (°)	Avg. res. (km)	Notes [R09: Rodriguez et al., 2009] [B10: Brown et al., 2010]
S22/T16 (22 July 2006)	~40°S	−38	20	58.6	31.5	59.3	77	Faint elongated streak The longitudinal extension seen in the dataset is larger than that of R09, but smaller than that of B10
	NP	57	All	N/A				Not detected by R09
S23/T17 (7 September 2006)	SP	−70	67	79.1	76.4	55.2	8.9	False detection by R09
	SP	−67	20	62.2	63.9	58.6	11.2	False detection by R09
	SP	−62	42	70	57.7	59.2	15	False detection by R09
	SP	−75	−20	N/A				Not detected by R09
	~40°S	−43	−38	28.4	65	63.8	52	Numerous small separated patches and streaks
	~40°S	−47	19	54.5	42.5	58.8	12	
	~40°S	−51	44	70.8	54.7	54.1	8	All detected by B10 as a unique large elongated streak
	~40°S	−45	45	73.5	38.5	61.9	36	
	~40°S	−45	32	63.3	40.1	59	14	
	NP	62	All	83.9	78	63	65	
S23/T18 (23 September 2006)	NP	55	All	72.5	82.5	64.3	63	
S24/T19 (9 October 2006)	SP	−76	All	73.1	76.3	64.8	46	
	~40°S	−45	4	50.1	25.2	64.9	40	Two distinct elongated streaks
	~40°S	−44	32	67.5	16.8	64.6	44	merged by B10 in a long and large cloud system
	NP	62	All	79.8	80.2	111	70	
S25/T20 (25 October 2006)	SP	−85	−85	70.8	70.7	65.3	12	Numerous small patches near the SP
	SP	−82	−30	65.8	60.8	65.8	12	
	SP	−85	2	71.2	61.2	65.4	12	
	SP	−77	−85	69.6	71.5	65.8	12	Merged by B10 in a large cloud system very near the SP
	SP	−78	22	67.8	50.4	65.3	12	
	SP	−76	40	71.1	52.5	65.1	12	
	SP	−65	−91	61.3	78.9	67.6	14	
	SP	−71	60	62.3	74.3	67.4	14	
	~40°S	−45	50	N/A				Not seen in the data Detected by B10 as a small patch very near the terminator
	~40°S	−31	−48	N/A				Extremely faint V-shaped streaks Not detected by R09 Merged by B10 in a large cloud system
	NP	60	All	76.3	80.3	114	81	
S26/T21 (12 December 2006)	SP	−85	−175	N/A				Not seen in the data Detected by B10 as a small patch very near the SP
	SP	−65	−88	N/A				Not seen in the data Detected by B10 as a very large patch extending from ~SP to 50°S latitudes
	~40°S	−48	45	72.6	15.3	67.6	27	System of large and thin streaks
	~40°S	−40	32	62.9	10.7	68.2	22	Merged by B10 in a unique huge cloud system. Haze artifact?
	~40°S	−35	−40	N/A				Faint cloud Not detected by R09
	TROP	−17	12	45.5	29.9	68.2	27	
	TROP	−15	−17	N/A				Not seen in the data Detected by B10 as a small patch
	NP	65	All	82.3	75	109.2	89	
S26/T22 (28 December 2006)	SP	−75	−105	N/A				Large patch extending up to the SP Not detected by R09
	SP	−66	15	N/A				Small patch Not detected by R09
	~40°S	−40	30	55.6	13.2	68.7	15.5	
	~40°S	−35	−37	N/A				Not seen in the data Detected by B10 as a long streak
	NP	57	All	74.4	77.5	113.8	90	
S27/T23 (13 January 2007)	SP	−87	All	77.9	40	73.9	25	

(*continued on next page*)

Table A1 (*continued*)

Sequence, Flyby # and date	Cloud type[a]	Avg. central lat. (°)	Avg. central East long. (°)	Mean inc. (°)	Mean em. (°)	Mean phase (°)	Avg. res. (km)	Notes [R09: Rodriguez et al., 2009] [B10: Brown et al., 2010]
	SP	−64.4	−54.4	52.9	50.9	74.7	37	Small patches Merged by B10 in a huge elongated cloud system too extended in latitudes and longitudes
	~40°S	−58.9	−14	47.8	35.8	74.7	36	
	~40°S	−44	45	72.4	6.1	74	27	One elongated streak and small patches
	~40°S	−47	17	54.6	20.5	74.6	41	Merged by B10 in a huge cloud system too extended in latitudes
	~40°S	−48.5	−9	41.2	35.8	74.8	38	
	~40°S	−32	−20	N/A				Not seen in the data Detected by B10 as a large cloud system extending from 45°S up to 5°S with very odd sharp edges. Artifact (borders of a VIMS image)
	NP	55	All	60.3	82.4	110.5	151	
S27/T24 (29 January 2007)	SP	−80	−70	68.9	47.8	74.9	15	Small patches Merged by B10 in a single cloud system
	~40°S	−39	10	43.2	34.1	77	12.5	Long annular cloud system Detected by B10 with a better shape than R09
	NP	56	All	73.4	63.5	105.1	78	
S28/T25 (22 February 2007)	NP	57	All	71.8	17.3	69.1	60	
S28/T26 (10 March 2007)	SP	−75	−175	N/A	Faint cloud near the SP.			Not detected by R09 Detected by B10 as a huge complex too extended in latitudes
	~40°S	−38	All	N/A				Faint annular cloud system Not detected by R09
	NP	75	All	87.9	30.8	60.8	29	Small bright patches embedded into a widespread, dimmer, cloud system
S28/T27 (26 March 2007)	SP	−85	174	N/A				Very faint small cloud right above the SP Not detected by R09
	SP	−65	70	N/A				Very faint small cloud Not detected by R09
	SP	−70	−132	70.1	55.1	125	45	
	~40°S	−46	−145	54.8	73.4	123.5	75	
	TROP	−5	117	N/A				Not seen in the data Detected by B10 as a very small patch
	NP	62	All	76.3	29.8	52	65	Small bright patches embedded into a widespread, dimmer, cloud system
S29/T28 (10 April 2007)	SP	−88	All	N/A				Very faint small cloud right above the SP Not detected by R09
	~40°S	−45	−134	62.5	78.5	130.8	69	Elongated streak and small patches Detected by B10 as a huge complex that expands too far in the south
	NP	55	All	69.4	29.7	45.1	35	Small bright patches embedded into a widespread, dimmer, cloud system
S29/T29 (26 April 2007)	SP	−73	All	62.5	78.5	139.5	96	
	TROP	−5	130	N/A				Very faint small cloud Not detected by R09
	NP	56	All	71.1	38.5	36.5	76	Small bright patches embedded into a widespread, dimmer, cloud system
S30/T30 (12 May 2007)	SP	−63	−118	52.7	79.8	144	92	Cloud detected by R09 near the limb. Uncertain. Data not used by B10
	~40°S	−56	130	50.5	76.5	29.8	83.5	
	NP	57	All	73.4	49.3	28.7	73	

Table A1 (*continued*)

Sequence, Flyby # and date	Cloud type[a]	Avg. central lat. (°)	Avg. central East long. (°)	Mean inc. (°)	Mean em. (°)	Mean phase (°)	Avg. res. (km)	Notes [R09: Rodriguez et al., 2009] [B10: Brown et al., 2010]
S30/T31 (28 May 2007)	~40°S	−51	110	58.6	75.7	25.1	61	
	~40°S	−52	127	55.5	73.7	25.1	62	
	NP	65.5	All	85.9	67.7	23.6	56	
S31/T32 (13 June 2007)	SP	−73	All	62.8	77.9	16	76	
	~40°S	−53	−158	60	75.5	15.6	65	Annular cloud system
	~40°S	−47	80	70.7	76.8	15.5	113	Detected by B10 with a better shape than R09
	NP	66.5	All	88.7	75.9	14.8	98	
S31/T33 (29 June 2007)	~40°S	−48	100	55.4	64.8	16.9	18	Very thin streaks and small patches
	~40°S	−50	118	49.6	59.6	16	18	Merged by B10 in a larger cloud system with an odd shape
	~40°S	−45	−178	48.3	59.3	12.3	118	
	NP	71	All	83.9	73.7	11.9	91	
S32/T34 (19 July 2007)								
	~40°S	−46	150	59.5	75.6	124.2	112	
	~40°S	−42	17	66.7	45.3	55.8	18	Thin streaks and small patches
	~40°S	−45	32	52.1	46.9	59.6	50	Merged by B10 in a larger and longer cloud system
	TROP	−25	175	N/A				Not seen in the data. Detected by B10 as a very small patch
	TROP	−10	150	N/A				Not seen in the data. Detected by B10 as a very small and thin streak
	NP	62.5	All	74	79.7	61.4	129	
S33/T35 (31 August 2007)	NP	60	All	75.5	65.3	27.7	28	
S34/T36 (2 October 2007)	~40°S	−53	110	70.3	65.3	32.6	82	Faint elongated patches
	~40°S	−46	−144	50.2	78.6	33	68	Detected by B10 as an almost complete annular belt at ~40°S, with a larger latitudinal extension than seen in the data
	TROP	−10	150	N/A				Not seen in the data Detected by B10 as a very small patch
	NP	58.5	All	77.1	79.4	32.6	92	
S35/T37 (19 November 2007)	~40°S	−50	−160	N/A				Very faint and small patch, right at the terminator. Uncertain
	NP	70	All	81.6	76.9	41.2	120	Not detected by R09
S35/T38 (5 December 2007)	SP	−66	−100	72.3	77.3	137	16	Long streak detected at high phase angle near the limb Not detected by B10
	~40°S	−50	115	N/A				Very faint, but large cloud Not as large as detected by B10 Not detected by R09.
	NP	60	All	76.6	76.2	44.9	142	
S36/T39 (20 December 2007)	~40°S	−49	−85	74.3	62.4	134	86	
	NP	71	All	82.8	58.4	50	102	
S36/T40 (5 January 2008)	SP	−68	−100	N/A				Not seen in the data
	~40°S	−45	−85	N/A				Detected by B10 at very high phase angle as very thin and small patches
	TROP	−16	−92	N/A				
	NP	60	All	77.3	69.1	57.5	66	
S38/T41 (22 February 2008)	TROP	−26	−98	62.5	57.5	119.5	69	
	NP	69	All	81.5	53.5	65.7	71	
S39/T42 (26 March 2008)	SP	−77	−160	69.2	69.1	109.6	15	
	~40°S	−50	−125	N/A				Not seen in the data Detected by B10 at very high phase angle as a large streak
	~40°S	−37	−80	N/A				Not seen in the data Detected by B10 at very high phase angle as very small patches
	TROP	−25	−115	47.3	72.8	111.7	98	
	TROP	−22	−80	80.9	32.1	110.2	21	Thin streaks and patches
	TROP	−25	−80	80.8	31.5	110.1	21	All merged by B10 in a larger cloud system. Haze artifact?
	TROP	−17	−72	88.6	24.3	110	22	

(*continued on next page*)

Table A1 (*continued*)

Sequence, Flyby # and date	Cloud type[a]	Avg. central lat. (°)	Avg. central East long. (°)	Mean inc. (°)	Mean em. (°)	Mean phase (°)	Avg. res. (km)	Notes [R09: Rodriguez et al., 2009] [B10: Brown et al., 2010]
	NP	66	All	76.7	58.3	73.6	99	
S40/T43 (12 May 2008)	SP	−80	−110	N/A				Not seen in the data Detected by B10 as very small patches very near the SP
	SP	−67	−172	61.2	75.3	102.6	79	
	~40°S	−37	−125	41.8	63.6	103	84	Small patches All merged by B10 in a larger cloud system too extended in latitudes and longitudes. Haze artifact?
	~40°S	−40	−90	N/A				Not seen in the data Detected by B10 as small patches
	TROP	−11	−105	51.2	56.9	102.8	74	
	NP	66	All	74.7	58.4	82.1	83	
S40/T44 (28 May 2008)	SP	−81	−41	87.6	54.9	94	48	Small patch Not detected by B10
	SP	−80	−98	79.2	55.4	94.3	54	Large patch Not detected by B10
	~40°S	−41	−93	63.8	34.8	95.7	100	Small patch Not detected by B10
	~40°S	−44	134	61.7	77.4	89.2	42	Large patch Not detected by B10
	TROP	−16	−93	65.5	30.9	93.5	33	Small patches Not detected by B10
	NP	81	All	89.8	63.3	88.5	64	One central cap encircled by an annular faint cloud
	NP	62	All	75.5	51.8	88.9	71	All merged by B10 in a larger cloud system too extended southward in latitudes (down to 35°N). Haze artifact?
S42/T45 (31 July 2008)	SP	−88	All	84.4	64.6	86.4	136	
	NP	74	All	84.8	59.3	96.8	75	
S45/T46 (3 November 2008)	~40°S	−37	−159	35.7	72	81.6	64	
	NP	62	All	71.7	52	94.8	110	One central cap encircled by an annular faint cloud
	NP	83	All	89.3	58.4	94.5	112	
S45/T47 (19 November 2008)	NP	61	All	70.9	63.5	100.3	97	One central cap encircled by an annular faint cloud
	NP	83	All	88	58.2	100.2	113	
S46/T48 (5 December 2008)	SP	−77	146	81.4	64.9	77.3	79	
	~40°S	−41	171	48.5	80.3	76.1	23	
	NP	64	All	75.3	55.8	108.3	112	One central cap encircled by an annular faint cloud
	NP	82	All	87.5	54.5	108.2	116	
S46/T49 (21 December 2008)	~40°S	−42	−119	46.4	29.2	71.2	51	
	~40°S	−40	−100	60.6	10.6	70.8	18	
	~40°S	−34	−92	64	10.5	70.5	15	
	TROP	−12	−133	21.1	52.6	72.4	29	
	NP	73	All	81.3	50	110.3	96	One central cap encircled by an annular faint cloud
S47/T50 (7 February 2009)	NP	66	All	76.5	47.1	105.9	97	Faint annular cloud
S49/T51 (27 March 2009)	~40°S	−49	−157	47.6	44.4	75.2	65	
	~40°S	−47	−68	80.6	10.7	74.5	49	
	NP	65	All	75.3	43.7	106.2	99	One central cap encircled by an annular faint cloud
	NP	83	All	86.7	35.2	106.1	114	
S49/T52 (4 April 2009)	~40°S	−49	−21	57.6	53.1	73.8	59	
	~40°S	−52	28	52.8	39.1	74.1	59	
	~40°S	−46	47	66.4	50.1	71.9	100	
	NP	67	All	77.3	42.7	108.3	83	
S49/T53 (20 April 2009)	~40°S	−42	12	52.4	52.4	67.6	83	
	NP	70	All	78.6	36.3	80.2	368	
S50/T54 (5 May 2009)	NP	80	70	82.7	45.3	118.7	57	Patchy
S50/T55 (21 May 2009)	~40°S	−42	−7	50.5	37.3	52.3	137	
	~40°S	−42	30	48.5	35.4	52	157	
	~40°S	−43	70	55	12.8	54.6	37	
	TROP	−25	73	48	30.9	55.2	34	
	NP	80	All	84.5	41.8	121.3	125	One central cap encircled by an annular faint cloud
S50/T56 (6 June 2009)	~40°S	−44	41	52	20.7	44.2	111	
	~40°S	−43	−34	62.8	46.9	44.1	111	
	TROP	−26	−20	48.9	49.7	44.4	110	

Table A1 (*continued*)

Sequence, Flyby # and date	Cloud type[a]	Avg. central lat. (°)	Avg. central East long. (°)	Mean inc. (°)	Mean em. (°)	Mean phase (°)	Avg. res. (km)	Notes [R09: Rodriguez et al., 2009] [B10: Brown et al., 2010]
	TROP	−3	19	8.8	43.5	44.3	131	Large diffuse patch very near the equator
	NP	71	57	72.5	61.3	130.2	82	Patchy.
S51/T57 (22 June 2009)	∼40°S	−39	−21	50.9	29.8	36.3	81	
	∼40°S	−40	24	49	21.8	36.5	71	
	∼40°S	−38	78	55.8	29.7	36.4	71	
	∼40°S	−52	96	75.4	44.5	36.1	67	
	NP	79	36	80.3	59.3	138.6	76	Patchy
S51/T58 (8 July 2009)	∼40°S	−52	−22	68.3	48.2	28.4	49	
	∼40°S	−44	−7	54.3	33.9	28.2	67	
	∼40°S	−43	72	53.1	28.8	30.3	30	
	∼40°S	−44	102	75.7	55.4	28.7	41	
	NP	79	40	80.3	68.1	148.1	52	Patchy
S52/T59 (24 July 2009)								
S52/T60 (9 August 2009)								
S53/T61 (25 August 2009)	∼40°S	−45	50	47	42.9	11.1	24	
	∼40°S	−46	14	50.4	41	11.8	52	
S54/T62 (12 October 2009)	∼40°S	−44	33	46.5	45.3	10.9	57	
	∼40°S	−44	−12	60.9	53.6	10.2	61	
	∼40°N	31	−6	43.3	39.7	10.4	98	
	∼40°N	31	4	43.5	39.5	10.4	98	
	NP	69	50	69.5	73.9	10.8	103	Patchy
S55/T63 (12 December 2009)	∼40°S	−47	140	60	53.7	48.1	47	Huge system, also constituted of some small patches and E–W elongated streaks
	∼40°S	−40	162	65.7	44.4	48.5	33	
	∼40°N	46	−176	82.3	56.6	46.1	56	
	∼40°N	47	178	76.3	53.1	46.2	57	
	NP	71	−120	77	76	45.7	86	Patchy
S56/T64 (28 December 2009)	∼40°S	−52	−178	81.2	53.1	42.8	36	
	∼40°S	−−50	70	52.7	59.6	48.1	386	
	NP	68	160	72.6	79.6	44.6	75	Patchy
S56/T65 (12 January 2010)	∼40°S	−50	172	69.5	49	43.2	50	
	∼40°S	−52	150	65.7	48.1	43.3	56	
	TROP	−14	90	22.6	58.9	44.4	62	
	NP	68	150	74.5	75.2	43.8	124	Patchy
S57/T66 (28 January 2010)	∼40°S	−54	89	59.7	62.1	38.6	16	
	∼40°S	−53	61	68.7	78.9	39.2	17	
	∼40°S	−58	148	71.2	56.1	43.1	75	
	∼40°S	−49	169	79.5	53	42.3	63	
	∼40°S	−45	165	78.7	49.7	42.6	69	
	∼40°S	−44	81	54.8	52.5	38.1	9	
	∼40°S	−34	89	42.2	53.2	39.1	12	
	NP	69	150	75.6	75.5	44.3	124	Patchy
S59/T67 (5 April 2010)	NP	74	10	74.1	78.3	16.4	94	Patchy

[a] SP: cloud detected very near the south pole or at southern high latitudes (poleward of 60°), ∼40°S: cloud detected at southern mid-latitudes (between −60° and −30°), TROP: cloud detected near equator (in a band comprise between −30° and 30°), ∼40°N: isolated cloud detected at northern mid-latitudes (between 30° and 60°), NP: large cloud detected near the North Pole (poleward of 55°).

identified and clearly stated in Rodriguez et al. (2009), due to the deliberate choice of conservative thresholds of detection. The consequences on the global mapping of Titan's clouds over 3.5 years including more than 140 cloud detections are minor and, in the end, this does not change any of the conclusions of Rodriguez et al. (2009) study. During this checking process, we also found a few systematic errors in the manual detection of Brown et al. (2010). In particular, we found that they missed 9 clouds (5.5% of total), and that their manual selection overestimates the spatial extent of 9 clouds (5.5% of total) and, on 10 occasions, merges numerous small individual clouds into a larger unique event (equivalent of missing 19 other clouds (11.6% of total)). We also found 19 (11.6% of total) false or uncertain detections. At the end, ∼80% of the 135 Brown et al. (2010) detections are found to be accurate both in shape and location. The method used by Brown et al. (2010) is more sensitive than the one of Rodriguez et al. (2009), as it allows them to miss fewer clouds. At the same time it appears to be too sensitive due to the inherent subjectivity of a pure visual inspection. The details of each detection consistency are given in Table A1. We can thus confirm 139 of the total 163 detections (a total of 163 minus 5 and 19 uncertain detections from Rodriguez et al. (2009) and Brown et al. (2010) respectively). This finally gives a rate of good detections of 95% ([143 − 6 − 5] = 132 over 139 confirmed clouds) for the semi-automated survey of Rodriguez et al. (2009) and 77% ([135 − 9 − 19] = 107 over 139 confirmed clouds) for the visual examination of Brown et al. (2010), proving the quality of the two studies. Moreover, more than 75% of the total 163 clouds referenced in Table A1 between July 2004 and July 2008 are jointly detected by Brown et al. (2010) and Rodriguez et al. (2009), indicating that both studies are very close. Both studies produced at the end almost the same global distribution and time evolution of the cloud coverage.

We also notice that Fig. 6 in Brown et al. (2010) is misleading. The cluster of VIMS flybys of Titan between October 2004 and January 2006 that they show in this figure is wrong. During this period, Cassini flew by Titan eight times, against only six in Brown et al. (2010) figure. Moreover a cluster of five targeted flybys between October 2004 and April 2005 is erroneously shifted by 6 months in Brown et al. (2010) figure. By correcting all these errors, the Fig. 6 of Brown et al. (2010) becomes very similar to the

Fig. 3a of Rodriguez et al. (2009) which also illustrates the time evolution of cloud latitude.

It should be noted that the algorithm developed by Rodriguez et al. (2009) to detect Titan's clouds has the advantaging of producing identical results every time, given the same dataset and detection criteria.

References

Adamkovics, M., Wong, M.H., Laver, C., de Pater, I., 2007. Widespread morning drizzle on Titan. Science 318, 962–965.

Adamkovics, M., de Pater, I., Hartung, M., Barnes, J.W., 2009. Evidence for condensed-phase methane enhancement over Xanadu on Titan. Planet. Space Sci. 57, 1586–1595.

Aharonson, O., Hayes, A.G., Lunine, J.I., Lorenz, R.D., Allison, M.D., Elachi, C., 2009. An asymmetric distribution of lakes on Titan as a possible consequence of orbital forcing. Nat. Geosci. 2, 851–854.

Atreya, S.K. et al., 2006. Titan's methane cycle. Planet. Space Sci. 54, 1177–1187.

Baines, K.H. et al., 2005. The atmospheres of Saturn and Titan in the near-infrared first results of Cassini/VIMS. Earth Moon Planet 96, 119–147.

Barnes, J.W. et al., 2005. A 5-micron-bright spot on Titan: Evidence for surface diversity. Science 310, 92–95.

Barnes, J.W. et al., 2006. Cassini observations of flow-like features in western Tui Regio, Titan. Geophys. Res. Lett. 33, L16204.

Barnes, J.W. et al., 2007. Global-scale surface spectral variations on Titan seen from Cassini/VIMS. Icarus 186, 242–258.

Barnes, J.W. et al., 2008. Spectroscopy, morphometry, and photoclinometry of Titan's dunefields from Cassini/VIMS. Icarus 195, 400–414.

Barnes, J.W. et al., 2009. VIMS spectral mapping observations of Titan during the Cassini prime mission. Planet. Space Sci. 57, 1950–1962.

Barth, E.L., Rafkin, S.C.R., 2007. TRAMS: A new dynamic cloud model for Titan's methane clouds. Geophys. Res. Lett. 34. doi:10.1029/2006GL028652.

Bouchez, A.H., Brown, M.E., 2005. Statistics of Titan's south polar tropospheric clouds. Astrophys. J. 618, L53–L56.

Brown, M.E., Bouchez, A.H., Griffith, C.A., 2002. Direct detection of variable tropospheric clouds near Titan's south pole. Nature 420, 795–797.

Brown, M.E. et al., 2009. Discovery of lake-effect clouds on Titan. Geophys. Res. Lett. 36, L01103.

Brown, M.E., Roberts, J.E., Schaller, E.L., 2010. Clouds on Titan during the Cassini prime mission: A complete analysis of the VIMS data. Icarus 205, 571–580.

Brown, R.H. et al., 2004. The Cassini Visual and Infrared Mapping Spectrometer investigation. Space Sci. Rev. 115, 111–168.

Brown, R.H. et al., 2008. The identification of liquid ethane in Titan's Ontario Lacus. Nature 454, 607–610.

Coustenis, A. et al., 2001. Images of Titan at 1.3 and 1.6 μm with adaptive optics at the CFHT. Icarus 154, 501–515.

de Pater, I. et al., 2006. Titan imagery with Keck adaptive optics during and after probe entry. J. Geophys. Res. 111, E07S05. doi:10.1029/2005JE002620.

Flasar, F.M., 1998. The composition of Titans atmosphere: A meteorological perspective. Planet. Space Sci. 46, 1109–1124.

Fulchignoni, M. et al., 2005. In situ measurements of the physical characteristics of Titan's environment. Nature 438, 785–791.

Gibbard, S.G. et al., 1999. Titan: High resolution speckle images from the Keck telescope. Icarus 139, 189–201.

Gibbard, S.G. et al., 2004. Speckle imaging of Titan at 2 microns: Surface albedo, haze optical depth, and tropospheric clouds 1996–1998. Icarus 169, 429–439.

Griffith, C.A., Owen, T., Miller, G.A., Geballe, T.R., 1998. Transient clouds in Titan's lower atmosphere. Nature 395, 575–578.

Griffith, C.A., Hall, J.L., Geballe, T.R., 2000. Detection of daily clouds on Titan. Science 290, 509–513.

Griffith, C.A. et al., 2005. The evolution of Titan's mid-latitude clouds. Science 310, 474–477.

Griffith, C.A. et al., 2006. Evidence for a polar ethane cloud on Titan. Science 313, 1620–1622.

Griffith, C.A. et al., 2009. Characterization of clouds in Titan's tropical atmosphere. Astrophys. J. 702, L105–L109.

Hayes, A.G. et al., 2010. Bathymetry and absorptivity of Titan's Ontario Lacus. J. Geophys. Res. 115, E09009. doi:10.1029/2009JE003557.

Hirtzig, M. et al., 2006. Monitoring atmospheric phenomena on Titan. Astron. Astrophys. 456, 761–774.

Hirtzig, M. et al., 2007. Titan: Atmospheric and surface features as observed with Nasmyth adaptive optics system near-infrared imager and spectrograph at the time of the Huygens mission. J. Geophys. Res. 112, E02S91.

Hueso, R., Sanchez-Lavega, A., 2006. Methane storms on Saturn's moon Titan. Nature 442, 428–431.

Janssen, M.A. et al., 2009. Titan's surface at 2.2-cm wavelength imaged by the Cassini RADAR radiometer: Calibration and first results. Icarus 200, 222–239.

Jennings, D.E. et al., 2009. Titan's surface brightness temperatures. Astrophys. J. 691, L103–L105.

Kim, S.J., Trafton, L.M., Geballe, T.R., 2008. No evidence of morning or large-scale drizzle on Titan. Astrophys. J. 679, L53–L56.

Lebonnois, S., Rannou, P., Hourdin, F., 2009. The coupling of winds, aerosols and chemistry in Titan's atmosphere. Philos. Trans. Roy. Soc. A 367, 665–682. doi:10.1098/rsta.2008.0243.

Le Corre, L. et al., 2009. Analysis of a cryolava flow-like feature on Titan. Planet. Space Sci. 57, 870–879.

Lemmon, M.T., Karkoschka, E., Tomasko, M., 1993. Titan's rotation – Surface feature observed. Icarus 103, 329–332.

Le Mouélic, S. et al., 2008a. Imaging of the north polar cloud on Titan by the VIMS imaging spectrometer onboard Cassini. Lunar Planet. Sci. XXXIX, 1649 (abstract).

Le Mouélic, S. et al., 2008b. Mapping and interpretation of Sinlap crater on Titan using Cassini VIMS and RADAR data. J. Geophys. Res. 113, E04003.

Le Mouélic, S. et al., 2011. Dissipation of Titan's north polar cloud at northern spring equinox. Planet. Space Sci. doi:10.1016/j.pss.2011.04.006.

Mace, G.G. et al., 2009. A description of hydrometeor layer occurrence statistics derived from the first year of merged Cloudsat and CALIPSO data. J. Geophys. Res. 114, D00A26. doi:10.1029/2007JD009755.

Mitchell, J.L., Pierrehumbert, R.T., Frierson, D.M.W., Caballero, R., 2006. The dynamics behind Titan's methane clouds. Proc. Natl. Acad. Sci. USA 103, 18421–18426.

Mitchell, J.L., Pierrehumbert, R.T., Frierson, D.M.W., Caballero, R., 2009. The impact of methane thermodynamics on seasonal convection and circulation in a model Titan atmosphere. Icarus 203, 250–264.

Mitri, G., Showman, A.P., Lunine, J.I., Lorenz, R.D., 2007. Hydrocarbon lakes on Titan. Icarus 186, 385–394.

Newman, C.E., Richardson, M.I., Lee, C., Toigo, A.D., Ewald, S.P., 2008. The TitanWRF model at the end of the Cassini prime mission. American Geophysical Union (Fall). Abstract #P12A-02.

Porco, C.C. et al., 2004. Cassini imaging science: Instrument characteristics and anticipated scientific investigations at Saturn. Space Sci. Rev. 115, 363–497.

Porco, C.C. et al., 2005. Imaging of Titan from the Cassini spacecraft. Nature 434, 159–168.

Radebaugh, J. et al., 2007. Mountains on Titan observed by Cassini RADAR. Icarus 192, 77–91.

Radebaugh, J. et al., 2011. Regional geomorphology and history of Titan's Xanadu province. Icarus 211, 672–685. doi:10.1016/j.icarus.2010.07.022.

Rannou, P., Montmessin, F., Hourdin, F., Lebonnois, S., 2006. The latitudinal distribution of clouds on Titan. Science 311, 201–205.

Rannou, P., Cours, T., Le Mouélic, S., Rodriguez, S., Sotin, C., Drossart, P., Brown, R., 2010. Titan haze distribution and optical properties retrieved from recent observations. Icarus 208, 850–867.

Rodriguez, S. et al., 2006. Cassini/VIMS hyperspectral observations of the HUYGENS landing site on Titan. Planet. Space Sci. 54, 1510–1523.

Rodriguez, S. et al., 2009. Global circulation as the main source of cloud activity on Titan. Nature 459, 678–682.

Roe, H.G., de Pater, I., Macintosh, B.A., McKay, C.P., 2002. Titan's clouds from Gemini and Keck adaptive optics imaging. Astrophys. J. 581, 1399–1406.

Roe, H.G., Bouchez, A.H., Trujillo, C.A., Schaller, E.L., Brown, M.E., 2005a. Discovery of temperate latitude clouds on Titan. Astrophys. J. 618, L49–L52.

Roe, H.G., Brown, M.E., Schaller, E.L., Bouchez, A.H., Trujillo, C.A., 2005b. Geographic control of Titan's mid-latitude clouds. Science 310, 477–479.

Schaller, E.L., Brown, M.E., Roe, H.G., Bouchez, A.H., 2006a. A large cloud outburst at Titan's south pole. Icarus 182, 224–229.

Schaller, E.L., Brown, M.E., Roe, H.G., Bouchez, A.H., Trujillo, C.A., 2006b. Dissipation of Titan's south polar clouds. Icarus 184, 517–523.

Schaller, E.L., Roe, H.G., Schneider, T., Brown, M.E., 2009. Storms in the tropics of Titan. Nature 460, 873–875.

Smith, P.H., Lemmon, M.T., Lorenz, R.D., Sromovsky, L.A., Caldwell, J.J., Allison, M.D., 1996. Titan's surface, revealed by HST imaging. Icarus 119, 336–349.

Soderblom, L.A. et al., 2007. Topography and geomorphology of the Huygens landing site on Titan. Planet. Space Sci. 55, 2015–2024.

Sotin, C. et al., 2005. Release of volatiles from a possible cryovolcano from near-infrared imaging of Titan. Nature 435, 786–789.

Stofan, E.R. et al., 2007. The lakes of Titan. Nature 445, 61–64.

Tokano, T., 2005. Meteorological assessment of the surface temperatures on Titan: Constraints on the surface type. Icarus 173, 222–242.

Tokano, T., 2008. Dune-forming winds on Titan and the influence of topography. Icarus 194, 243–262.

Tokano, T., 2009. Impact of seas/lakes on polar meteorology of Titan: Simulation by a coupled GCM-sea model. Icarus 204, 619–636.

Tokano, T., Neubauer, F.M., 2002. Tidal winds on Titan caused by Saturn. Icarus 158, 499–515.

Tokano, T., Neubauer, F.M., 2005. Wind-induced seasonal angular momentum exchange at Titan's surface and its influence on Titan's length-of-day. Geophys. Res. Lett. 32, L24203.

Tokano, T., Neubauer, F.M., Laube, M., McKay, C.P., 2001. Three-dimensional modeling of the tropospheric methane cycle on Titan. Icarus 153, 130–147.

Tomasko, M.G. et al., 2005. Rain, winds and haze during the Huygens probe's descent to Titan's surface. Nature 438, 765–778.

Toublanc, D., Parisot, J.-P., Brillet, J., Gautier, D., Raulin, F., McKay, C.P., 1995. Photochemical modeling of Titan's atmosphere. Icarus 113, 2–26.

Turtle, E.P. et al., 2009. Cassini imaging of Titan's high-latitude lakes, clouds, and south-polar surface changes. Geophys. Res. Lett. 36, L02204.

Yung, Y.L., Allen, M., Pinto, J.P., 1984. Photochemistry of the atmosphere of Titan – Comparison between model and observations. Astrophys. J. Suppl. Ser. 55, 465–506.

Wall, S. et al., 2010. Active shoreline of Ontario Lacus, Titan: A morphological study of the lake and its surroundings. Geophys. Res. Lett. 37, L05202.

Zebker, H.A., Stiles, B., Hensley, S., Lorenz, R., Kirk, R.L., Lunine, J.I., 2009. Size and shape of Saturn's moon Titan. Science 324, 921–923.